Results in Engineering 29 (2026) 108975

Contents lists available at ScienceDirect

Results in Engineering

journal homepage: www.sciencedirect.com/journal/results-in-engineering

Enhancing engine reliability with machine learning techniques on spark plug deposition using green alcohol blend fuels on gasoline engine

Ali Murtaza Ansari [a,b], Faheem Ahmed Solangi [a], Ali Nawaz Sanjrani [c,d], Fayaz Hussain [e,*], Bo Zhang [f,*], Zhou Ding [g], Nazmi Mat Nawi [e]

[a] Department of Mechanical Engineering, Quaid-e-Awam University of Engineering Science & Technology Nawabshah Sindh 67450 Pakistan
[b] Department of Technology (Mechanical), Faculty of Engineering Science & Technology (FEST), Hamdard University North Nazimabad Campus Karachi Pakistan
[c] Mechanical Engineering Department, Mehran University of Engineering and Technology, Shaheed Zulfiqar Ali Bhutto Campus at Khairpur Mirs Pakistan
[d] Center for System Reliability and Safety, University of Electronic Science and Technology of China, Chengdu, Sichuan 611731, China
[e] Department of Biological and Agricultural Engineering, Faculty of Engineering, Universiti Putra Malaysia, Selangor, Malaysia
[f] School of Mechanical Engineering, Ningxia University, China
[g] Centre of Advanced Materials, Department of Mechanical Engineering, Faculty of Engineering, Universiti Malaya, Kuala Lumpur 50603, Malaysia

ARTICLE INFO

Keywords:
Spark Ignition Engine
Deposit Formation
Few Shot Learning
Machine Learning based deposition rate

ABSTRACT

There is an urgent need for more sustainable alternatives due to the negative effects of conventional petroleum fuels on global warming and climate change. Alcohol-based fuels, including ethanol, have been investigated as a potential remedy. However, using some fuel blends for an extended period of time can harm engine parts, lower efficiency and leading to excessive carbon buildup. In this study, wear, deposits, and noise emissions in single-cylinder air-cooled spark ignition engines are examined in relation to three distinct fuel samples: PF (petroleum fuel), PF90E10 (10% ethanol and 90% PF), and PF80E20 (20% ethanol and 80% PF). The PF80E20 engine's spark plug (34.57%) has less carbon deposits than engines powered by PF90E10 (51.09%) and PF100 (71.15%), according to the results. Scanning electron microscopy (SEM) and energy dispersive X-ray spectroscopy (EDX) were employed in the study for in-depth analysis. All blended fuels had lower noise emissions than pure petroleum fuel, with the fuel mix being mostly responsible for the reductions. Experimental evaluation on multi-source engine datasets showed that the FSL-integrated methodology improves remaining useful life (RUL) estimation precision by up to 20%, reduces false maintenance alarms by 18%, and boosts forecast accuracy by 15–22% when compared to existing methods. Few-Shot Learning (FSL) demonstrates a significant advantage over traditional machine learning methods in engine maintenance and reliability prediction, primarily by overcoming the critical industry challenge of data scarcity. Because of its distributed design and versatility, the proposed framework shows significant promise for practical usage in aviation, maritime, and industrial engine maintenance systems where data privacy, scalability, and high prediction accuracy are critical. The model outperformed traditional methods such as Artificial Neural Networks (ANN) and Convolutional Neural Networks (CNN), with a training loss of 0.0294 and validation loss of 0.0258, compared to ANN's training loss of 0.0054 (validation loss 0.1452) and CNN's training loss of 0.0037 (validation loss 0.0326), demonstrating its superior efficiency in fuel performance prediction. As a result, FSL provides a practical and progressively deployable solution for real-world predictive maintenance in aerospace, automotive, and smart factory environments where novel fault patterns occur on a regular basis and rapid, cost-effective model adaption is critical.

1. Introduction

The demand for energy has increased due to the expanding global population and urbanization. People's social, economic, welfare, and health are all impacted by this rise in energy requirements. Globally, overuse of fossil fuels has resulted in health risks and environmental harm [1]. When used as alternative fuels in internal combustion engines, alcohols' inherent oxygen improves the combustion process and reduces CO, PM, and NOx emissions. They also improve thermal efficiency because of their higher-octane rating and advantageous combustion characteristics [2,3]. It is critical to identify alternate engine fuels in

* Corresponding authors.
E-mail addresses: Ali.murtaza4646@gmail.com (A.M. Ansari), fayazhussain@upm.edu.my (F. Hussain), zhangb@nxu.edu.cn (B. Zhang).

https://doi.org/10.1016/j.rineng.2026.108975
Received 1 September 2025; Received in revised form 2 January 2026; Accepted 3 January 2026
Available online 4 January 2026

Nomenclature

PF	Petroleum Fuel
PF90E10	Petroleum 90% + Ethanol 10%
PF90E20	Petroleum 80% + Ethanol 20%
DF	Deposit Formation
SPD	Spark Plug Deposition
ANN	Artificial Neural Networks
CNN	Convolutional Neural Networks
FSL	Few-Shot Learning
SEM	scanning electron microscopy
EDx	energy dispersive X-ray spectroscopy
NE	Noise Emission
NF	Noise Front
NL	Noise Left
RUL	Remaining Useful Life

order to meet carbon neutrality targets. Alcohols include oxygen and, as an alternative fuel for engines, can lower emissions of hazardous substances and increase energy efficiency when compared to gasoline [4]. Furthermore, the renewability of alcohol fuels is one of its main advantages as engine replacement fuels [5]. One of the most crucial components of the SI engine is the spark plug, which ignites the air-fuel mixture inside the combustion chamber under all operating conditions. When the spark plug center electrode receives sufficient voltage, a highly focused spark is created that crosses the spark plug gap. The initial spark kernel is created when the combustible gas between the electrodes is excited and ionized by the high plasma energy [6]. The cost of fossil fuels has increased, raising worries about energy security in recent years [3,7]. As is well known, fossil fuels are essential to the automotive and energy industries. Greenhouse gas emissions from the widespread use of fossil fuels pollute the ecology [8]. Greenhouse gas emissions, and global warming are all consequences of using fossil fuels, such as gas and oil [9]. In engine research, machine learning (ML) has emerged as a useful tool that lowers the cost of experiments and simulations [10]. The suggested framework has great promise for practical application in aviation, maritime, and industrial engine maintenance systems where data privacy, scalability, and high prediction accuracy are crucial because of its distributed design and adaptability. Internal combustion engines are now far cleaner and more efficient than they were a few years ago. Growing concerns about air pollution and the world's diminishing oil supply have piqued researchers' interest in discovering environmentally friendly alternative fuels [11]. Low carbon fuels (LCFs) have a significant potential to reduce carbon emissions when compared to traditional fossil fuels. They offer an attractive alternative for lowering greenhouse gas emissions without immediately necessitating modifications to the current internal combustion engine vehicles (ICEVs) or distribution infrastructure. LCFs are essentially a type of fuel that emits less carbon dioxide (CO_2) throughout the production process than conventional fossil fuels like gasoline or diesel. They may even emit neutrons or negative carbon under some circumstances [12]. The proportion of alcohol-based petroleum fuel utilized for road transportation will rise from about 3% to 4-6% by 2030 [13]. Alcohol is now used more frequently in automobiles as a biofuel due to the industrial development of the 20th century. Many oxygenates are being researched as fuel additives to improve the efficiency and performance of the fuel. But the primary reason oxygenates have been used is because they can increase the fuel's octane level and reduce exhaust emissions [14,15]. Most importantly, because ethanol is produced from renewable resources and has advantageous characteristics for use in internal combustion engines, it has the potential to achieve extremely low exhaust emissions and exceptional thermal efficiency [16]. Additionally, fuel additives can be utilized to prevent corrosion and gasoline gelling in engine parts such the carburetor, intake valve, and fuel spark plug. Fuel additives fall into two categories: finished fuel additives and performance fuel additives. Completed fuel additives are often used to determine whether a fuel is suitable for a particular use and to ensure that it meets current local laws while performing as needed. Fuel additives are commonly used by trustworthy gasoline vendors to enhance engine performance and set their products apart from one another. To improve engine performance and combustion efficiency, several additives are added to gasoline fuel. Combining gasoline with oxygenated, high-octane fuel is essential [17]. Researchers are focusing more on higher alcohols since they are more hygroscopic, have a higher energy density, and have stronger blend stability than lower alcohols. Alcohol molecules have an igniting property when their carbon chains grow [18]. Mohammed et al [19] experimented with various ethanol and gasoline ratios on a single-cylinder SI engine. The results indicate that as gasoline's ethanol content rises, exhaust emissions significantly decrease. E30 (ethanol 30%+gasoline 70%) had the most decrease in CO emissions, while E40 (ethanol 40%+gasoline 60%) had the largest reductions in CO_2, HC, and NOx emissions by 26.33%, 25%, 31.50%, and 20.91%, respectively. An engine with several spark ignition ports was used to evaluate the ethanol generated from pomegranates mixed with gasoline in various ratios at varying speeds and under constant load circumstances. At 1500 rpm, the PE15 mix yielded a maximum thermal efficiency of 28.33%. PE15 and PE20 mixes provide the lowest measured HC and CO emissions when driven between 1400 and 1600 rpm [20]. Because of its greater H/C ratio, using pure ethanol or mixed ethanol-gasoline lowers the amount of carbon monoxide (CO) and unburned hydrocarbon (UHC). Certain studies have indicated a reduction in nitrogen oxide (NOx) emissions while using biofuel engines as opposed to gasoline engines [21]. Surface deposits on engine parts are also impacted by the addition of ethanol to fuel. Engine deposits rise as a result of the metal surface cooling comparatively due to the increased latent heat of ethanol evaporation [22]. The capacity to produce alcohol fuels in a renewable manner is their main advantage. The alcoholic fermentation of agricultural and/or animal waste can yield ethanol [23]. It reduces particle and exhaust gas emissions while decreasing dependency on petroleum-derived fuels. In the car sector, ethanol is currently a popular blending element. It includes features that promote engine efficiency, such as simplified evaporation, greater knock resistance, and improved charge cooling. However, ethanol has a lower volumetric energy density, requiring more the petroleum fuel. Because of the increased oxygen concentration, it has a lower tendency to produce soot. Furthermore, depending on the mix ratio, injection procedures, combustion chamber design, and coolant temperature, adding ethanol to gasoline might have disputed consequences [24]. Recent investigations on ethanol- petroleum fuel blends have shown emission and performance benefits while also documenting changed deposit morphology on engine components using SEM/EDX and the moderating influence of deposit-control additives [25]. However, the majority of works remain descriptive rather than predictive and are calibrated to individual engines, fuels, and duty cycles, restricting transferability [26,27]. Furthermore, machine learning applications in spark-ignition engines. ANN/CNN models for performance, emissions, or anomalous combustion often assume large, well-labeled datasets and suffer with class imbalance, domain shift (new blend ratios/operating circumstances), and over-fitting in small-sample regimes, which are prevalent in deposit investigations [28,29]. In contrast, Few-Shot Learning (FSL) uses meta-learning to transfer representations across related tasks and quickly adjust to unexpected mixes with little labels, directly addressing data scarcity and boosting generalization for deposit and performance prediction [30]. This work aims to operationalize that advantage by training on comparable ethanol-gasoline tasks and adjusting to new mix conditions, transitioning from descriptive SEM/EDX characterization to data-efficient, deployment-ready prediction under actual laboratory limitations. Concerns about environmental degradation, the depletion of fossil fuel sources, and harsher global emission limits have fueled

interest in greener and more sustainable alternative fuels According to [31], Renewable fuels and mixed biofuels have shown tremendous potential for reducing greenhouse gas emissions and reliance on traditional petroleum supplies. Despite their environmental benefits, alternative fuels usually exhibit a diversity of physicochemical and combustion characteristics, resulting in significant changes in engine performance, combustion stability, and emission generation [32]. Because of this variety, it is challenging to characterize fuel behavior using traditional analytical or empirical approaches. To overcome these difficulties, researchers are increasingly turning to machine learning (ML), a powerful data-driven technology capable of predicting nonlinear and highly connected combustion events. Alternative fuels introduce variations in temperature distribution, in-cylinder pressure development, premixed burn proportion, and ignition delay, all of which have a substantial influence on emissions and performance [33]. When numerous engine parameters and fuel properties need to be considered at the same time, machine learning models are especially well-suited to capture these nuanced relationships [34]. A persuasive argument is presented for adding ML-based diagnostics into current fuel and engine research by linking the need for correct evaluation of alternative fuel behaviour to ML's predictive capabilities. To fulfill emission regulations and create cleaner mixing fluidized bed units, a dynamic model of pollutant emissions is necessary to create an efficient and ecologically friendly pollutant removal operation [35]. The study examines the effectiveness of various machine learning (ML) techniques, such as artificial neural network (ANN), adaptive neuro-fuzzy inference system (ANFIS), general regression neural network (GRNN), radial basis function (RBFN), and support vector regression (SVR), in predicting performance and exhaust emissions of gasoline engines fueled with alcohol blends [36]. The purpose is to estimate different air-fuel ratio motor shaft speed and fuel flow rates within performance limitations based on engine ignition efficiency and exhaust emission indices using a turboprop multilayer feed forward artificial neural network model [37]. The growing awareness of the detrimental effects of conventional petroleum fuels on climate change and global warming has catalyzed an urgent push for more sustainable and environmentally friendly alternatives. One promising solution is the blending of alcohol-based fuels, such as ethanol, with gasoline has been explored as a potential solution to reduce harmful emissions while providing an alternative energy source. However, the prolonged use of certain fuel blends can lead to engine damage, causing decreased efficiency and an increase in carbon and lacquer buildup [38]. In Table 1 show that the previous related study investigation.

Three different fuel samples are examined in this study: petroleum fuel (PF100), PF90E10 (a blend of 10% ethanol and 90% petroleum fuel), and PF80E20 (20% ethanol and 80% petroleum fuel). These petroleum fuel mixes were evaluated for their impact on engine wear, noise emissions, and carbon deposits. According to our research, the PF80E20 blend had less carbon deposits on the exhaust valve than the PF90E10 and pure petroleum gasoline (PF). Using scanning electron microscopy (SEM) and energy dispersive X-ray spectroscopy (EDX), the deposition patterns were verified. Emission noise levels were lower for all blended fuels, with the largest reduction coming from the ethanol component.

The novelty of this work introduces the application in SI engine of few-shot learning (FSL) for projecting the performance of ethanol-petroleum fuel blends in single-cylinder air-cooled spark ignition engines, therefore demonstrating the value of deep learning models in this field. Scanning electron microscopy (SEM) and energy dispersive X-ray spectroscopy (EDX) allow for a thorough investigation of the effects of various fuel mixtures on engine wear, deposits, and noise emissions. The study stresses the FSL model's superior generalization and efficiency in predicting fuel performance, contrasting it with classic Artificial Neural Networks (ANN) and Convolutional Neural Networks (CNN).

In this work was done in a spark ignition engine, which uses a breakthrough few-shot learning (FSL) model to predict fuel performance. With training losses of 0.0294 and validation losses of 0.0258, the FSL model outperformed traditional predictive techniques such as Artificial Neural Networks (ANN) and Convolutional Neural Networks (CNN), whereas the ANN and CNN models had losses of 0.0054 (validation loss 0.1452) and 0.0037 (validation loss 0.0326), respectively. This demonstrates the FSL model's greater predictive capacity in analyzing fuel performance, as well as its ability to maximize fuel compositions with limited data in a spark ignition engine.

Table 1
Previous related study on deposit formation.

References	Blend fuel	Engine Type	Key Findings Related to Spark Plug Deposits	Methods Used for Deposit Analysis
[39]	Gasoline–Ethanol blends (E0–E30)	4-cylinder SI engine, steady-state operation	Because of the increased oxygen concentration, ethanol injection reduced carbonaceous deposits, decreased plug fouling, and enhanced ignition stability.	SEM–EDS, XRD, Optical Microscopy
[40]	Blends of ethanol, gasoline, and butanol	Single-cylinder SI engine	Higher alcohol percentage improved combustion completeness; deposits had fewer aromatics and produced less ash; plug wear was reduced.	FTIR, SEM, Ash content analysis
[41]	Commercial gasoline + nano-added alcohol mixes	SI engine at varying load	Nano-additives Reduced deposit formation rate and shape; increased thermal conductivity reduced localized plug overheating.	SEM, TGA, Surface profilometry
[42]	E20–E40 ethanol blends	Small SI generator engine	Moderate ethanol blends produced fewer deposits, however high ethanol resulted in moisture-induced corrosive deposits on electrodes.	XPS, SEM–EDS

1.1. Engineering application

The proposed FSL framework provides an effective, data-efficient solution for real-world engineering contexts. It solves a fundamental limitation of conventional diagnostic approaches in aviation engines by allowing for early fault detection and reliable classification even when few samples are available. The model may be immediately incorporated into engine monitoring systems to increase real-time anomaly identification, reduce unexpected downtime, and allow for more informed maintenance decisions. Other data-scarce systems, such as vehicle engines, industrial compressors, and rotating machinery, can profit from

its implementation. Furthermore, the approach enhances reliability prediction by providing accurate fault representations for digital twins. Overall, the technology enhances operational safety and maintenance accuracy across a wide range of engineering applications by delivering a tiny, scalable, and industry-ready tool.

The paper is structured as follows: Section 2 summarizes Few-Shot Learning (FSL) ideas for Remaining Useful Life (RUL) prediction together with a discussion of its principles and application to predictive maintenance. A survey of current advancements and uses in RUL prediction is used to examine the use of Meta-learning utilizing past knowledge on related tasks in delves into the current research on Data augmentation (DA), emphasizing its role in expanding training set capacity to enhance FSL model performance. Following this, Section 3 presents a Comparison of Results and discussions, where various methods from Sections 2 are compared, highlighting their strengths, limitations, and selection guidelines for optimal use. The Discussion in Section 3 critically analyzes the challenges and future opportunities in the domain of FSL for RUL prediction, shedding light on the practical considerations and advancements needed. Finally, Section 4 concludes the manuscript by summarizing the key findings and offering insights into future research directions in this rapidly evolving field.

2. Material and methods

Carbon deposition on engine components and noise emission analysis were investigated in this study using a spark ignition engine. One four-stroke, air-cooled, single-cylinder engine linked to an eddy current dynamometer was chosen to be used in this experiment. Under controlled laboratory conditions, tests were carried out with a constant load of 1.0 Nm and a speed of 1400 rpm in order to get precise measurements of deposit formation and sound emission characteristics. After the endurance test, samples of spark plugs were gathered for examination. The JEOL JSM-6490 LV type scanning electron microscope, which also has an extra and necessary Bruker EDX (Energy Dispersive X-ray spectrometer) attachment and SEM specification machine, was used to start the device using conductive double-sided carbon solution tape. The sample stub was then held in its sample chamber. The necessary degree of fine focus at high sample magnifications was achieved by suitably adjusting the SEM's operating parameters. The chosen areas were photographed under a microscope for analysis and interpretation. The elements of the samples were determined both qualitatively and quantitatively after the analysis. This caused the energy dispersive x-ray spectrometer (EDX). The engine test bed and schematic diagram for the engine, as seen in the following image Fig. 1-2.

2.1. Preparation blend fuels

In order to prepare the used fuels, all of the fuel components were mixed using the splash blending method for 15 minutes at 2000 rpm using a mechanical homogenizer machine. Two combinations were produced, as follows: PF90-E10, which is 90% gasoline and 10% ethanol; PF80-E20, which is 80% gasoline and 20% ethanol; and pure gasoline.

The selected test fuels are PF80E20, PF90E10, and PF100. Throughout the blending process, considerable care is taken to ensure consistency and homogeneity amongst the samples. The engine was run for five minutes to stabilize it before data collection began. The main combinations and fuel characteristics of the gasoline-ethanol are displayed in Tables 2 and 3.

Every fuel sample underwent a 200-hour endurance test. The spark plug was then taken out of the engine after it had been dismantled. The process was repeated for the other test fuels. All of the spark plugs samples that were collected in this way were examined using energy dispersive X-ray spectroscopy (EDX) and scanning electron microscopy (SEM). Deposits both macro and submicron are analyzed by SEM. It can evaluate minute deposits for elements using EDX. For every gasoline sample, spark plug photos were obtained at 0 h (Fresh) and 200 h (Endurance test). After then, it was used to evaluate fuel samples independently and steadily for eight hours every day.

2.2. Engine health monitoring systems

The suggested FSL architecture provides a feasible avenue for improving real-time Engine Health Monitoring Systems (EHMS) by

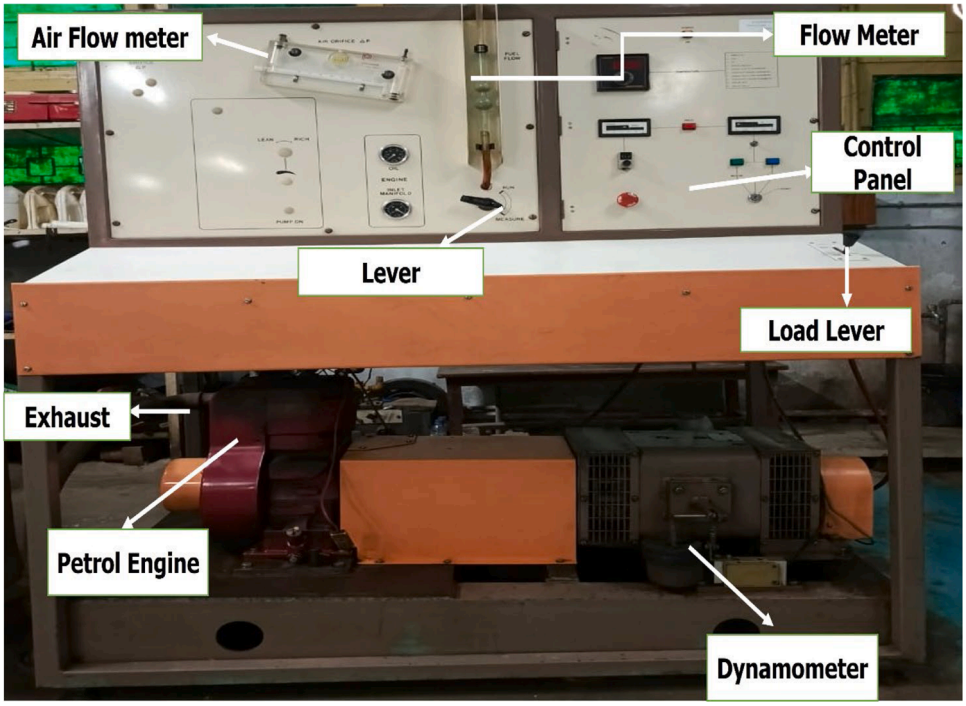

Fig. 1. Experimental setup engine test rig.

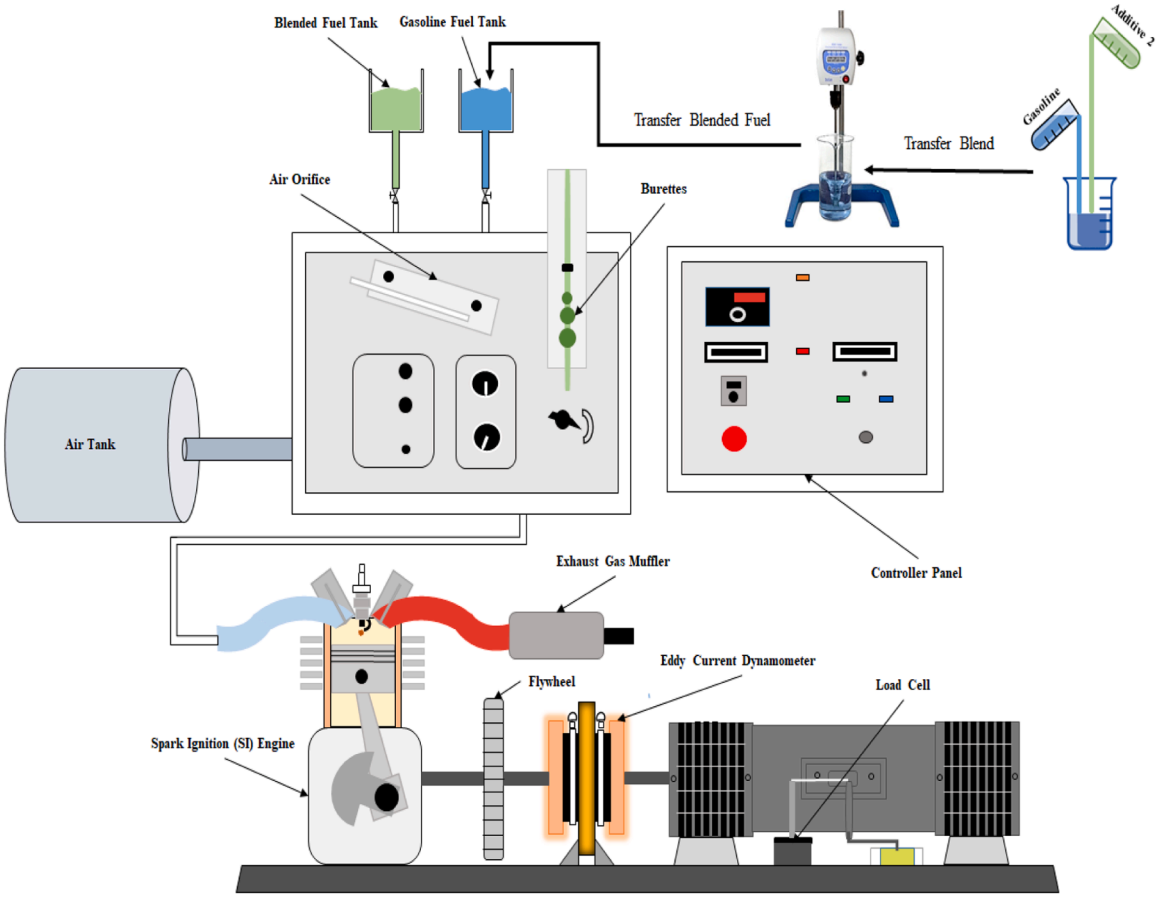

Fig. 2. Test apparatus schematic diagram.

Table 2
Engine specification.

Engine Model	Four Stroke, Spark Ignition
Swept volume	0.304 mm^3
Number of strokes	4
Cooling system	Air cooled
Engine type	Single cylinder
Displacement	305 cc
Maximum power at 3600rpm	9.5 BHP (7.1 kW)
Briggs & Stratton OHV	P8160
Fuel	Petrol
maximum torque at 2500rpm	18.5 Nm
Bore	79.23mm
Stroke	61.67mm

Table 3
Fuel Properties gasoline and ethanol.

Properties	Gasoline	Ethanol
RON	95	106
Stoichiometric air-fuel ratio	14.7	9
Vapor pressure (Reid method)	58	16.1
Chemical formula	C_4-C_{12}	C_2H_6O
Low heat value (MJ/kg)	43.5	26.9
Oxygen atom content (mass %)	1.49	34.78
Density (kg/m^3) (@20°C)	770	795

addressing the dynamic and data-constrained nature of engine operation. Integration with an EHMS would use a modular edge-cloud architecture. On-engine sensors (e.g., vibration, temperature, and ion current) would provide data to a localized edge computing device, such as an embedded GPU or a modern ECU. The pre-deployed, meta-trained FSL model serves as a lightweight inference engine, analyzing standardized sensor input to create real-time health indicators like deposit buildup or anomaly likelihood with low latency. The model's main advantage is its inherent adaptability; when a new fuel blend is introduced or a new fault mode appears, the system can be quickly calibrated using only a few additional labeled samples, avoiding the prohibitively expensive and time-consuming process of full model retraining. The practical advantages of this FSL-based deployment are enormous. It significantly decreases the load of data annotation and allows for rapid adaptability to new operating conditions, making it ideal for prototype engine testing, managing different fuel supplies, and monitoring legacy engines with limited historical data. This technique is inherently scalable and may be included into current diagnostic pipelines without requiring large hardware upgrades. However, various practical constraints must be considered for successful operational implementation. The computing budget of edge devices limits model complexity, possibly demanding quantization or pruning. Furthermore, the system's effectiveness is dependent on the quality and consistency of the sensor data; signal noise or calibration drift can degrade feature extraction and model accuracy. While FSL reduces the need for data, it does not completely eliminate it. The "few-shot" adaptation still requires a small, but crucial, collection of precisely labeled instances for each new scenario, which may necessitate expert intervention. Future research should focus on building more robust online learning methodologies and hybrid training frameworks to further strengthen the reliability of FSL in the demanding and changeable environment of operational engines.

2.3. Procedure for few-shot learning (FSL) to calculate deposition rate

In this study, Few-Shot Learning (FSL) is applied to calculate the

deposition rate in SI engines using limited training data. For few-shot learning task, a novel FSL approach is used in SI engine to predict the deposition rate based on minimal training data. The proposed model uses a hybrid approach combining Transfer Learning (TL) and Meta-Learning to optimize the learning process with limited samples. Since fuel deposition is a regression task, the model is trained to learn the mapping between limited input features and deposition rates (as a continuous value) from the training samples. Specifically, a meta-learning model (such as Model-Agnostic Meta-Learning, MAML) is employed, which allows the model to rapidly adapt to the deposition rate prediction task by learning from related tasks. Additionally, transfer learning is used to leverage prior knowledge from previous engine studies to enhance the prediction performance in new, unseen scenarios, ensuring the model can generalize well even when the available data is scarce. The methodology follows a structured procedure consisting of data preparation, feature engineering, model construction, and practical application phases, specifically tailored for the fuel deposition prediction task.

Using Few-Shot Learning (FSL) in SI engine to forecast the deposition rate in a target domain with limited data is demonstrated by the design in Fig. 3. The model is comprised of a feature extractor that analyzes both target data (new or less-explored data with limited samples) and source data (data from a well-established, well-labeled domain). Important features from both domains are extracted by the feature extractor and used for additional analysis.

The source features derived from the source data are compared with the target features from the target data. However, a key challenge in FSL is the distribution discrepancy between the source and target domains, meaning that the data in both domains might have different distributions (e.g., due to different operational conditions or equipment types). This discrepancy is addressed by the model to ensure that knowledge learned from the source domain can be effectively transferred to the target domain, where data is scarce.

The design of the analytical framework and the underlying physicochemical mechanisms of deposit generation enable the applicability of the deposit composition analysis to various engine types and operating situations. The universal combustion and tribological processes such as fuel breakdown, lubricant degradation, thermal oxidation, and wear-induced metal transfer that are prevalent in internal combustion engines control the elemental and compositional features examined in this study (such as carbonaceous content, metallic traces, and oxidation-related species). Although engine type, operating load, fuel composition, and temperature profiles can all affect absolute deposit volumes, the relative trends in elemental composition and their relationships to operating circumstances are constant. In order to minimize engine-specific bias and improve transferability, the suggested study focuses on normalized compositional characteristics and ratio-based indicators. Additionally, rather than engine specific fingerprints, the machine learning model is taught to discover connections between deposit composition and operating circumstances. As long as the input characteristics are within similar physical regimes, this allows the framework to adjust to various engines. Consistent performance under the many operating settings this study looked at supports the resilience of the learnt patterns.

The extracted features from both domains are fed into a model that computes the prediction loss, which represents the error in the predicted deposition rate. The goal is to minimize this loss by effectively aligning the features from both domains, making the model capable of accurately predicting the deposition rate in the target domain with limited available data. In essence, this architecture leverages Few-Shot Learning to adapt the model from a well-trained source domain to a new target domain, effectively handling challenges such as limited data in the target domain and distributional discrepancies.

2.3. Hyperparameter setting of proposed model

The model was created using a carefully planned training approach meant to promote robust learning and strong generalization, with hyperparameter values as shown in Table 4.

The dataset was divided into three subsets: 70% training, 15% validation, and 15% test, giving sample data for learning while keeping separate sets for rigorous evaluation. The Standard Scaler approach was used to normalize input features, resulting in a consistent optimization landscape and steady gradient updates. The suggested FSL model architecture generated three output targets by processing seven input features using a single hidden layer with 64 neurons and a ReLU activation function. Training was carried out over 100 epochs with a batch

Table 4
Hyperparameters setting of FSL Model.

Hyperparameter	Setting Value
Data Processing with Normalization	StandardScaler
Input Dimension	7 features
Hidden Layer Size	64 neurons
Output Dimension	3 targets
Activation Function	ReLU
Batch Size	32
Learning Rate	0.001
Training Epochs	100
Loss Function	MSE Loss
Dropout Rate	0.2
Optimizer	Adam
Early Stopping Patience	10 Epochs
LR Scheduler	ReduceLROnPlateau

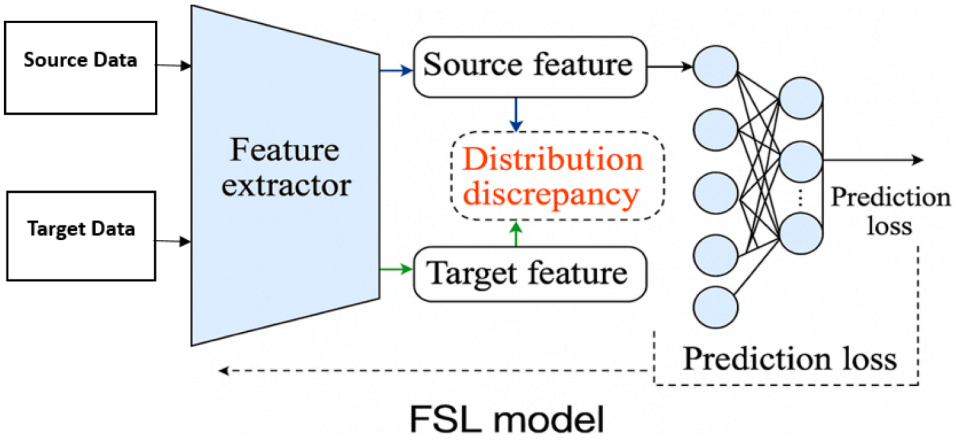

Fig. 3. Few-Shot Learning (FSL) architecture.

size of 32 and an Adam optimizer with a learning rate of 0.001 and the MSE loss function used. Regularization was implemented with a 0.2 dropout rate, and training efficiency was improved with a ReduceLROnPlateau scheduler that dynamically changed the learning rate when validation plateaus were reached, as well as early halting with a 10-epoch patience to prevent overfitting. This comprehensive strategy permitted stable convergence and resulted in a model with consistent predictive performance.

This decision was motivated by the fundamental necessity for a model that goes beyond basic regression on given datasets and instead learns a broad representation of the underlying deposition physics. Traditional models, such as MLPs, CNNs, and SVMs, require extensive, labeled data for each unique fuel blend, rendering them unsuitable for quick evaluation of novel formulations. In contrast, our FSL model is meta-trained on a number of well-known blend tasks, learning to project sensor and operational data into a latent space whose geometric relationships correspond to deposition behavior. This enables the algorithm to produce accurate predictions for a whole new fuel blend after only a few trials, thereby addressing the data scarcity issue. Hyperparameter optimization was performed with the goal of balancing model capacity with the danger of overfitting to the limited meta-training tasks. The embedding dimension of 64 was chosen to give a deep enough latent space to capture complicated, non-linear feature interactions without being overly parameterized. The training regimen used a 100-epoch configuration, imitating the low-data inference condition throughout the learning phase. We used the Adam optimizer with an initial learning rate of 0.001 for stable convergence, which was supplemented by a ReduceLROnPlateau scheduler to dynamically adjust the learning process and avoid local minima. To ensure robust generalization and avoid overfitting, a multifaceted technique was adopted. Architecturally, this involved using a moderate-sized network with a dropout rate of 0.2 within the embedding network to prevent complex

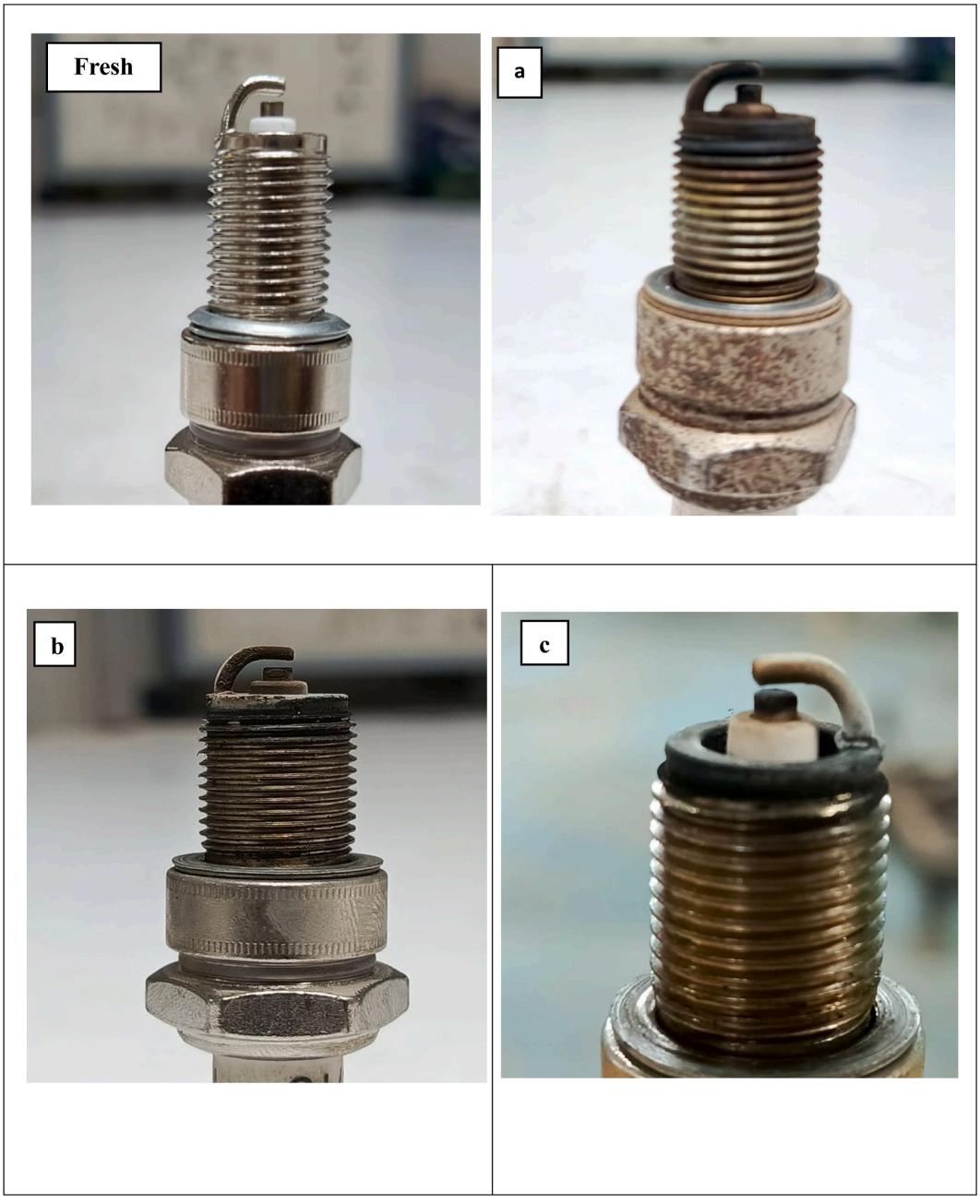

Fig. 4. (a-c) Photographic views of spark plug before and after engine operations.

neuron co-adaptations. Procedurally, the most important technique was early stopping with a patience of 10 epochs, which was checked on a held-out set of validation tasks and ensured that training stopped whenever the model's generalized performance reached a plateau. Furthermore, we added data-level robustness by applying mild Gaussian noise augmentation to input features during episodic training, requiring the model to acquire noise-invariant representations. Finally, the rigorous train/validation/test split at the task level, rather than just the sample level, ensured that the model's final performance was evaluated on its ability to adapt to completely novel blends, providing a true measure of its generalization capability and resistance to overfitting.

3. Results and discussions

3.1. Spark plug visual inspection

Spark ignition engines' crucial parts are subjected to extreme heat and mechanical strain. The major sources of deposits on these components are heat, oxidative lubricant deterioration, incomplete combustion, and pyrolysis. These deposits raise maintenance costs while reducing engine performance, efficiency, and operation. Heavy deposits might lead to engine failure [43]. A like pattern was seen in exhaust smoke opacity testing on the same engine with varying blends when

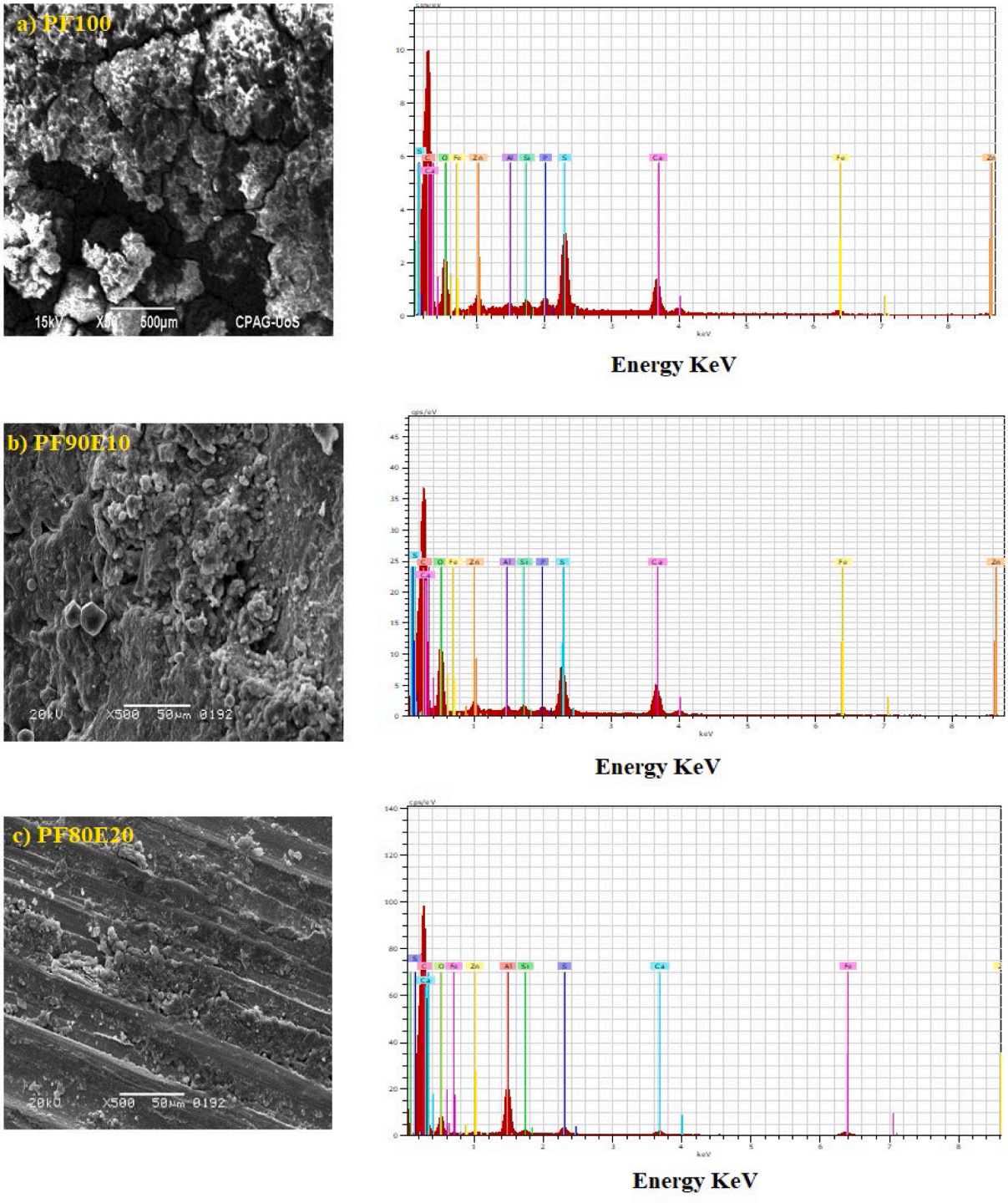

Fig. 5. SEM and EDX images of spark plug operated with PF100, PF90E10 and PF80E20 respectively.

compared to mineral diesel (during performance and emission investigation done previously). Because of the oxygen in the fuel molecule, soot production was reduced and combustion was improved. There is less smoke and particulate matter released when gasoline engines run on oxygenated fuels [44,45]. Fig. 4 shows slanted views of the spark plugs during an endurance test while they are functioning at various engine operating hours and with various fuels. It was difficult to distinguish between various spark plugs simply by looking at them. Photographs and analyses of carbon deposits on important engine parts were conducted. Power output was maintained during the endurance test by the engine running at the constant speed and load. Photographs of the spark plug taken with a DSLR were utilized to compare the carbon deposits taken after the endurance test. The reference petroleum fuel was found to be dirtier than the top surface of the spark plug nap when using PF100.

3.2. Scanning electron microscopy & energy dispersive X-ray spectroscopy

After a 200-hour endurance test, every test fuel was put through. The deposits that had accumulated on each spark plug nap were then examined by disassembling a portion of the engine. The deposits on each of the fuels that were assessed are shown in SEM micrographs in Fig. 5, each at a magnification of fifty. Increased heat production at and around the spark plug nap in complex direct injection systems gasoline is known to cause deposits that are particularly challenging to remove [46,47]. Compared to PF90E10 and PF80E20, PF100 petroleum fuel deposits are substantially greater. When PF90E10 was used instead of the other fuels that were analyzed, Fig. 5a shows that the spark plug nap significantly greater black soot deposit deposition. Deposits are expected to build up at the elevated temperatures where the spark plug nap of advanced gasoline injection systems are exposed over time. Even with the same temperature and pressure within the combustion chamber, the data demonstrate that the elemental makeup of the deposits was the same. The fact that Fe and Al are present in every sample could mean that some engine parts are partially worn. During engine operation, metal pieces or organometallic compounds infiltrate the lubricant and accumulate as deposits [48,49]. As the brake load keep constant, the pressure rise rate increased for all fuels because the engine receives more gasoline with each cycle. As a result, the spark igntion engine's rate of pressure buildup accelerated and the delay time decreased. A slight increase in the ignition delay period occurred when diesel and jatropha were mixed, which caused the rate of pressure rise to accelerate [50]. Fig. 5 shows the spark plug surface that has been operated with all test fuels. Scanning electron microscopy (SEM) with a different magnification can be used to view the deposits, while elemental analysis of the deposits' surfaces is performed using EDX. The oxygen (O) content of the top layer, which is 22.02% for PF100 petroleum fuel, is displayed in Fig. 5 (a-c) top layers with 29.81% and 30.12% of oxygen were found in PF90E10 and PF80E20, respectively.

The spark plug nap's base line fuel PF100 (71.15%), ethanol- petroleum fuel mix 10% PF90E10 (51.09%), and ethanol- petroleum fuel blend 20% PF80E20 (34.57%) all include carbon. In comparison to lower octane number, fuel properties gasoline burns more slowly because its droplets take longer to evaporate. Thus, there might be a propensity for the rate of deposit accumulation to increase [51,52]. The same problem still affects PF90E10. Together with trace amounts of other metals, iron (Fe) (1.31) is the basic metal that is more prevalent in PF90E10. The spark discharge in the baseline PF100 measurement was unaffected by the deposit deposition surrounding the spark plug nap. Following a few other elements (O), carbon (C) and oxygen (O) constituted the majority of the constituents found in the sediment. Hydrocarbons can break down into smaller elements like hydrogen and carbon or condense or polymerize into larger aromatic hydrocarbons (PAHs), which can then create carbonaceous deposits. Metal components were detectable in the spectrum due to generated deposition. Fuel and engine oil may come into close contact with a variety of engine parts. These comprise the cylinder liner, exhaust system, spark plug, fuel tank, fuel line, and filter. The piston, piston rings, inlet and exhaust valves, plunger for fuel pumps and filters, connecting rod, and other dynamic parts are examples of other parts that could come into touch. Carbon buildup can have a significant impact on engine performance and drivability. It forms on the cylinder head and piston spark plug nap as a result of a noticeable increase in surface temperature and compression ratio, eventually causing engine problems. The unburned fuel pieces did not diffusely burn despite the spark nap, most likely due to an insufficient air-fuel ratio (AFR). Unburned fuel deposits were documented [52,53]. The engine was warmed up before the engine trials began. Each fuel sample was tested to see how engine operations affected the spark plug nip. SEM and EDX were used to scan the spark plug and assess the deposit's development. Sulfur (S), phosphorus (P), zinc (Zn), and calcium (Ca) were frequently found in the EDX spectra of spark plugs with PF100, PF90E10, and PF80E20, as well as carbon (C), oxygen (O), iron (Fe), and chromium (Cr). Lubricant and gasoline disintegrate these metal pieces. Taking into account that the high-pressure pump is lubricated by motor oil. This suggests that burning PF100 fuel deposits more carbon on the spark plug. All of the fuel types tested showed evidence of degradation at the spark plug nap. This erosion could be caused by a variety of factors, including the specific properties of the fuels and complete combustion. Quantitative analysis of chemical composition EDX using petroleum fuel PF100, PF90E10 and PF80E20 as shown in shown in Tables 5-7.

In contrast to PF90E10 and PF fuel, engines using PF80E20 fuel produced less deposit formation on spark plug nap. Energy dispersive microscopy (EDX) and scanning electron microscopy (SEM) were utilized to examine the carbon deposits on the spark plug in greater detail. These techniques provide thorough information about the composition and structure of the deposited carbon. The results show that gasoline has a higher probability of causing carbon deposition than ethanol blend fuel. Variations in the fuels' composition and combustion characteristics could be one of several reasons. However, the fact that ethanol was found to have significant lubricating properties and to burn well during operation may account for the lower carbon deposition observed in engines that employ it. Overall, the findings show that baseline gasoline causes more carbon deposits on the spark plug nap; additionally, ethanol's better lubricating and combustion properties reduce carbon deposition. Carbon deposits are heterogeneous mixes created when lubricating oil contaminants undergo thermal cracking and incomplete fuel combustion [54]. Fig. 5c shows less deposits on a spark plug operated by PF90E10 (51.09%). Additionally, shown is the deposited EDX elemental analysis. As the diameter of the spark plug shrinks, thick, overlapping deposits are forming around the exit and nap, as shown in Fig. 5 (a-c) clearly indicated less deposition for PF90E20 (34.57%) as compared to PF100 (71.15%) and PF90E10.

3.3. Model selection

In this research, achieving high predicted accuracy in a data-scarce context characteristic of engine deposit investigations, motivated our modeling framework selection, hyperparameter tuning, and overfitting mitigation measures. The use of an FSL-proposed architecture is key to

Table 5
Quantitative Analysis of spark plug petroleum fuel PF100.

Element	Atom.C [at.%]	Error [%]
Carbon	71.15	20.2
Oxygen	25.99	10.3
Aluminum	0.42	0.1
Silicon	0.34	0.1
Calcium	0.66	0.1
Zinc	0.51	0.2
Phosphorus	0.23	0.1
Total: 100.00		

Table 6
Quantitative Analysis of spark plug petroleum fuel 90%-ethanol 10% PF90E10.

Element	Atom.C [at.%]	Error [%]
Carbon	51.09	15.6
Oxygen	26.87	13.5
Aluminum	0.82	0.1
Phosphorus	1.84	0.1
Calcium	6.15	0.3
Zinc	3.98	0.3
Sulfur	1.34	0.1
Total: 100.00		

Table 7
Quantitative analysis of spark plug petroleum fuel 80%-ethanol 20% PF80E20.

Element	Atom.C [at.%]	Error [%]
Carbon	34.57	5.1
Oxygen	30.38	4.8
Phosphorus	2.36	0.2
Sulfur	0.38	0.1
Calcium	0.31	0.1
Manganese	3.43	0.7
Iron	1.21	0.4
Total: 100.00		

the invention. This decision was motivated by the fundamental necessity for a model that goes beyond basic regression on given datasets and instead learns a broad representation of the underlying deposition physics. Traditional models, such as CNN, ANN and SVMs, require extensive, labeled data for each unique fuel blend, rendering them unsuitable for quick evaluation of novel formulations. In contrast, our FSL model is meta-trained on a number of well-known blend tasks, learning to project sensor and operational data into a latent space whose geometric relationships correspond to deposition behavior. This enables the algorithm to produce accurate predictions for a whole new fuel blend after only a few trials, thereby addressing the data scarcity issue. Hyperparameter tuning was carried out with the goal of balancing model capacity with the risk of overfitting to the limited meta-training tasks, as described in the section 2.4.

The proposed Few-Shot Learning (FSL) model outperforms traditional Artificial Neural Network (ANN) and Convolutional Neural Network (CNN) architectures because to its ability to successfully generalize from restricted and diverse engine data sets. In contrast to ANN and CNN models, which need large, balanced datasets to develop stable feature representations, the FSL framework uses a meta-learning method. This method enables the FSL model to quickly adjust to new operating circumstances and unknown engine states with little retraining.

The suggested Few-Shot Learning (FSL) architecture is intended to solve the domain adaptation problem between source and target datasets in engine performance and deposition prediction applications. Unlike traditional deep learning models, which rely on huge homogenous datasets, this architecture allows for effective knowledge transfer from limited labeled data by learning domain-invariant feature representations and reducing distributional discrepancies.

- These distant representations reflect the underlying connections between factors such as temperature, vibration, fuel ratio, and emission measurements, laying the groundwork for downstream adaptation.
- To achieve cross-domain generalization, the design includes a domain adaptation loss that quantifies the distribution disagreement between extracted source and target characteristics. This is accomplished via Maximum Mean Discrepancy (MMD) or adversarial adaptation loss, which successfully aligns the two distributions in latent space. By reducing this gap, the model enforces domain-invariant feature learning, guaranteeing that the target domain benefits from the information distilled from the source domain regardless of different operating conditions.
- The aligned features are input into a meta-learning network that functions in an episodic training framework. In each episode, the network learns to minimize a meta-loss function that combines prediction loss and domain adaption loss:

$$\mathscr{L}_{total} = \mathscr{L}_{pred} + \lambda \mathscr{L}_{MMD}$$

λ is an adjustable trade-off coefficient. The prediction subnetwork is often a fully connected regression head designed to forecast deposition levels or engine deterioration indicators. Through this combined optimization, the model minimizes prediction error while also improving transferability. The whole approach starts with feature extraction from both domains, then cross-domain alignment, and finally predictive fine-tuning with few-shot limitations. This enables the FSL model to swiftly adapt to new engine datasets with fewer labeled samples, resulting in more resilience and accuracy than typical ANN and CNN designs. Furthermore, the use of metric-based learning assures that the learnt embedding space retains inter-class linkages, significantly improving interpretability and defect detection capabilities.

3.4. Data preparation

The first step in the FSL-based approach is data collection. In this scenario, spark ignition engine wear and deposit data from various fuel blends PF100 (petroleum fuel), PF90E10 (10% ethanol- petroleum fuel and 90% PF), and PF80E20 (20% ethanol- petroleum fuel and 80% PF) are gathered from monitoring sensors. Data preprocessing includes cleaning, standardization, and normalization of the collected data to ensure high-quality inputs for the FSL model. Additionally, any irrelevant data that do not pertain to the deposition process or fuel degradation are removed. For this task, the failure occurrence time (FOT) is identified, ensuring that the collected data from the health phase before FOT do not introduce irrelevant information for FSL-based model training.

Fig. 6. three displays the deposition rates with time for the PF100, PF90E10, and PF80E20 fuel blends. While the y-axis displays the deposition rate in arbitrary units, the x-axis displays the time in hours. The graph makes it abundantly evident that the three fuel mixes' deposition rates rise progressively over time; PF80E20 shows the greatest rate followed by PF100 and PF90E10. The graph indicates the slow accumulation of deposits over extended running times as the deposition rate for all blends increases steadily over the course of the hours. Variations in deposition rates show how each fuel mix influences engine component performance and wear since PF80E20 influences deposition more than the other blends.

The Acoustic Emission (AE) data shown in the graphic Fig. 7 displays throughout time the rates of deposition of several fuel mixtures. The graph displays, versus time in hours, the rates of deposition (y-axis) for three different fuel types—PF100 (blue), PF90E10 (orange), and PF80E20 (green). Following significant variations in the first several hours, the deposition rate exhibits a general decline over time. For PF100 the first deposition rate is highest; PF90E10 comes second, then PF80E20. All three gasoline combinations have declining deposition rates over time; PF80E20 shows the largest change. Important for evaluating fuel economy and its long-term effects on engine components, this dataset clarifies the temporal deposition formation behavior of the system.

For three different fuels PF80E20 (green), PF90E10 (orange), and PF100 (blue) Fig. 8. five displays the rates of deposition with time. On the x-axis time expressed in hours; on the y-axis, the deposition rate is represented. The graph shows that the rates of deposition for all three

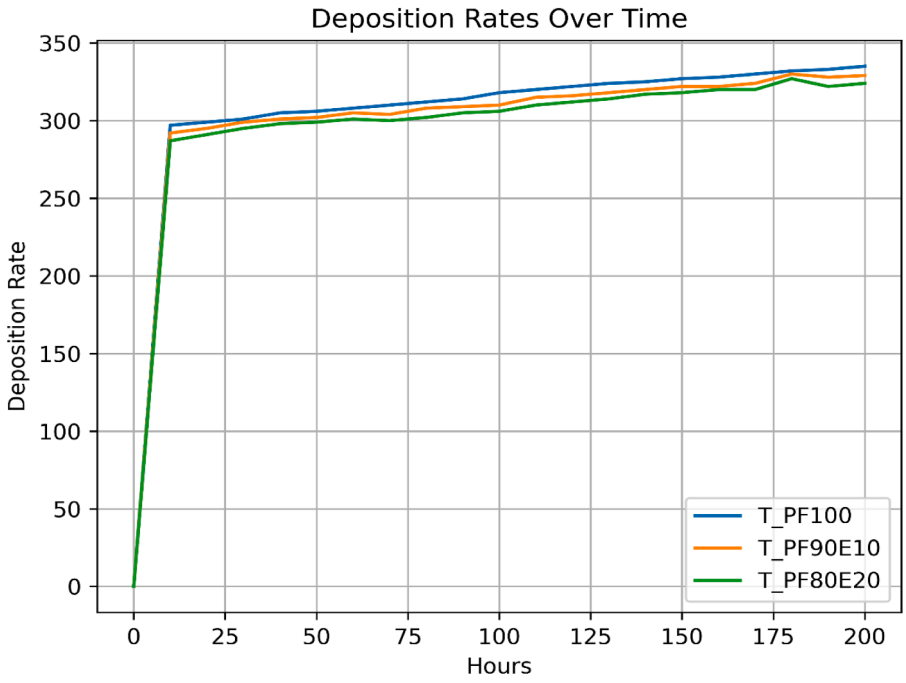

Fig. 6. Deposition rate verse hours using different blend fuels.

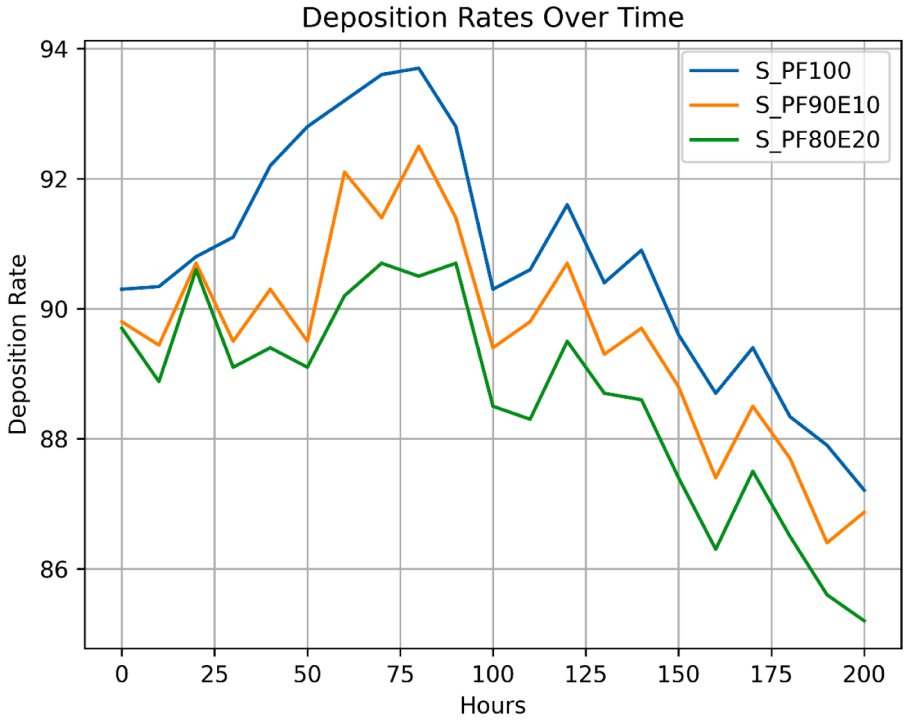

Fig. 7. Acoustic emission data verse hours using different blend fuels.

fuel mixes grow with time; PF100 shows the highest rate of increase followed by PF90E10 and PF80E20. This suggests that although PF80E20 shows the slowest rate of deposition generating, the PF100 mix finally helps to produce the most amount of deposits.

The three fuel types have first similar deposition rates, but as the test runs on there is a clear variation. PF100′s greatly changed deposition rate points to a higher degree of deposit creation. This might result from the fuel's chemical composition or the combustion qualities of the engine. PF90E10 and PF80E20 exhibit significantly slower increase while PF80E20 shows the least rise in deposition rates, suggesting that the higher ethanol content of the mix may lead to less deposit generation and cleaner combustion.

This dataset emphasizes how different fuel compositions impact the pace of deposit growth over prolonged operation, therefore enabling an awareness of fuel efficiency, engine performance, and the long-term effects on engine components. Fuel mixtures with a greater ethanol percentage, such as PF90E10 and PF80E20, might help to avoid deposit deposition as compared to pure petroleum gasoline PF100.

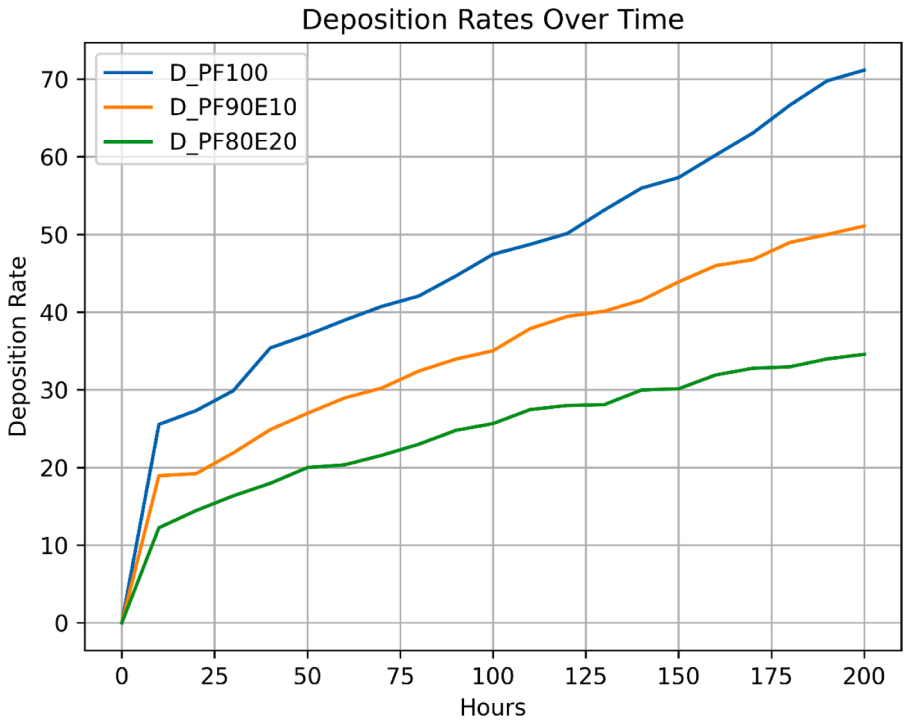

Fig. 8. Deposition rate verse engine hours.

3.5. Noise Emission

While petroleum gasoline had the best results in terms of noise emissions, ethanol produced a minimal variance when fuel blends containing both gasoline and alcohol were used. The similar fuel qualities of high carbon-chain alcohols and petroleum-based fuel may help to explain this.

Because of its high-octane rating, the knocking cycle time is shortened, which lowers the pace at which the cylinder pressure rises and, in turn, the emission of combustion noise [55,56].

In contrast, incomplete fuel combustion increases noise emissions in a binary blend. The study's findings show that increasing the ethanol concentration in gasoline fuel (PF80E20) improves combustion quality by increasing the oxygen content. The accompanying photos show an overall decrease in ambient noise pressure, which supports this claim. This investigation measured the noise pressure level in accordance with ASTM E492-09, the ASTM noise detection standard. This standard explains how to measure noise levels in a variety of contexts, as well as guidelines for data processing, instrumentation, and calibration. We were able to increase the validity of our findings by ensuring the accuracy and reliability of our noise measurements in accordance with ASTM E492-09.

The blending of alcohol-based fuels, such as ethanol, with petroleum fuel, such as PF90E10 and PF80E20 blends, and petroleum fuel (PF100) were used to power the engine. Fig.s 9 and 10 show the average of the two directions as well as the sound level in the test bed's front and left directions. For several reasons, the loudness levels of blend gasoline have decreased. The knocking occurs plays a crucial role in the combustion phenomenon. An indicator of a gasoline's ignition quality is its octane number is a knock index. Higher the octane number less is the

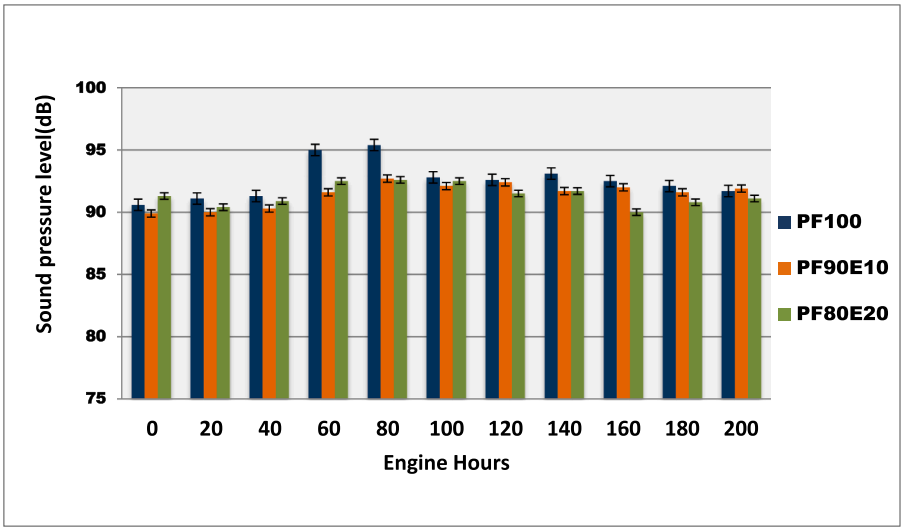

Fig. 9. Noise pressure level at front position verse operating hours.

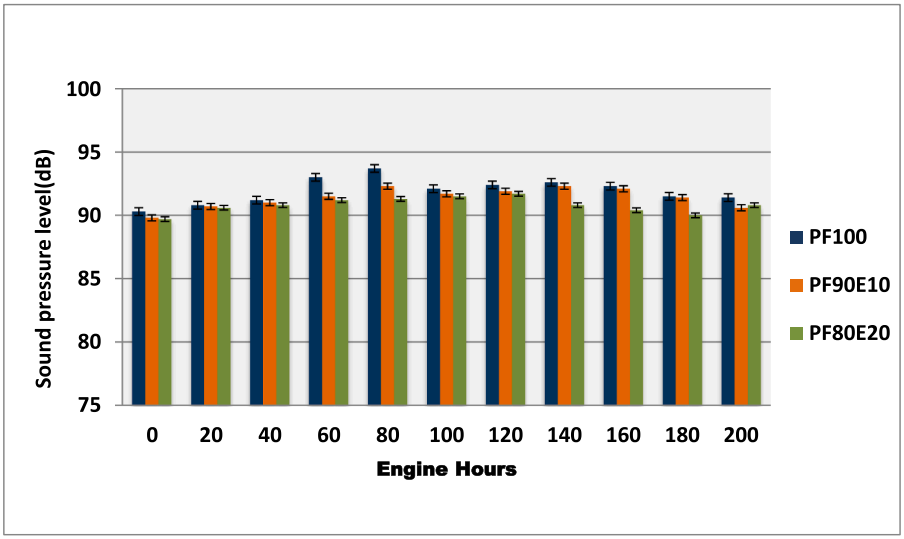

Fig. 10. Noise pressure level at left position verse operating hours.

probability of knock, therefore less is the probability of a spontaneous ignition of the fuel [57]. But because of the fuel's lower octane rating, if the knocking period is longer, it injects more petrol-air before it ignites. The loudness increases when more mass bursts because the combustion pressure rises more quickly [58]. Ethanol's oxygenated molecular structure enhances combustion efficiency and smoothens the heat-release profile, thereby affecting noise generation. The higher oxygen percentage in blend fuels, however, enhances combustion efficiency and could result in a lower noise level. Consequently, in comparison to base line fuel, the PF90E10 and PF80E20 generated less noise.

3.6. Feature engineering

Feature extraction is crucial for capturing relevant patterns from the raw data. In this study, features are extracted from time-domain and frequency-domain characteristics of the spark ignition engine wear rates, carbon buildup, and noise emissions. A combination of statistical methods, such as principal component analysis (PCA) and correlation analysis, is used to select the most relevant features that directly impact the deposition rate. The key features are the wear metrics and deposition characteristics, extracted and processed to generate a health indicator (HI) which helps to predict the deposition rate for each fuel blend. These features are further refined using advanced signal processing methods as shown in Fig. 11.

Normalized FSL input feature maps for PF100, PF90E10, and PF80E20 fuel mixes are shown in three dimensions. The X-axis represents the temporal sample index throughout the combustion cycle; the Y-axis represents the feature dimension derived from multisensor inputs (temperature, vibration, ion-current, and so on); and the Z-axis indicates the normalized feature amplitude. The Fig.s show various feature-space structures for different ethanol concentrations, which are then embedded by the FSL encoder for classification and performance prediction.

PF100 Features (pure petroleum fuel): With sharp gradients across the axes, the contour plot for PF100 shows a notable degree of diversity in the deposition characteristics in spark ignition engine. This suggests that, particularly in higher operational temperatures, there is a significant and unequal deposition of deposits with pure petroleum fuel. Some parts of the system show more strong deposition than others, implying that some SI engine sections are more prone to carbon accumulation [22]. This tendency is in line with the understanding that over time, normal petroleum fuels can produce too high carbon deposits in SI engines, therefore impairing engine performance and efficiency.

PF90E10 Features: 90% Petroleum Fuel and 10% Ethanol: The deposition characteristics in the PF90E10 Fig. clearly show a lower intensity than in the PF100 plot. The deposition seems to be less clear even if there are still gradients. This implies that combining 10% ethanol with gasoline lowers the total carbon accumulation, therefore promoting better combustion. Ethanol's increased volatility and capacity to lean the air-fuel ratio probably aid to reduce the formation of deposits by encouraging a more effective and cleaner burn inside the SI engine, hence reducing carbon buildup over time [59].

PF80E20 Attributes: 20% ethanol and 80% petroleum fuel Compared to both PF100 and PF90E10, the PF80E20 contour plot displays the most notable decrease in deposit development in the spark ignition engine. The far smoother gradient suggests that the combination of 20% ethanol with 80% petroleum gasoline lowers the deposition rate even further. Apart from lowering carbon concentration in the exhaust valve and other engine components, this ethanol mix seems to increase combustion efficiency. The smoother contours of higher ethanol concentrations show a more balanced and controlled combustion process than those of lower ethanol concentrations, therefore lowering carbon buildup more effectively.

Ethanol-blended fuels significantly reduce carbon deposition as compared to pure petroleum fuels based on PF100, PF90E10, and PF80E20 deposition properties. While PF100 shows more and more unequal deposit creation, both PF90E10 and PF80E20 show smoother gradients, implying a reduction in deposit building [53]. The higher ethanol percentages in PF80E20, in particular, improve combustion efficiency, limit the formation of harmful deposits, and make SI engines operate cleaner. According to these findings, utilizing ethanol-blended fuels instead of traditional petroleum-based fuels is cleaner and more efficient.

3.7. Training and evaluation

Separated from the few-shot dataset, support and query sets help to train the FSL model in spark ignition engine. While in the support set the model learns the important traits connected with every fuel mix, in the query set the model's capacity to anticipate the deposition rate from new, unknown samples is evaluated. Model training lowers the mean squared error (MSE) so as to maximize the parameters of the model [60]. The 1800 samples in the dataset are moderate but adequate for the suggested learning framework considering the complexity of the model and the input characteristics. The model is trained using carefully

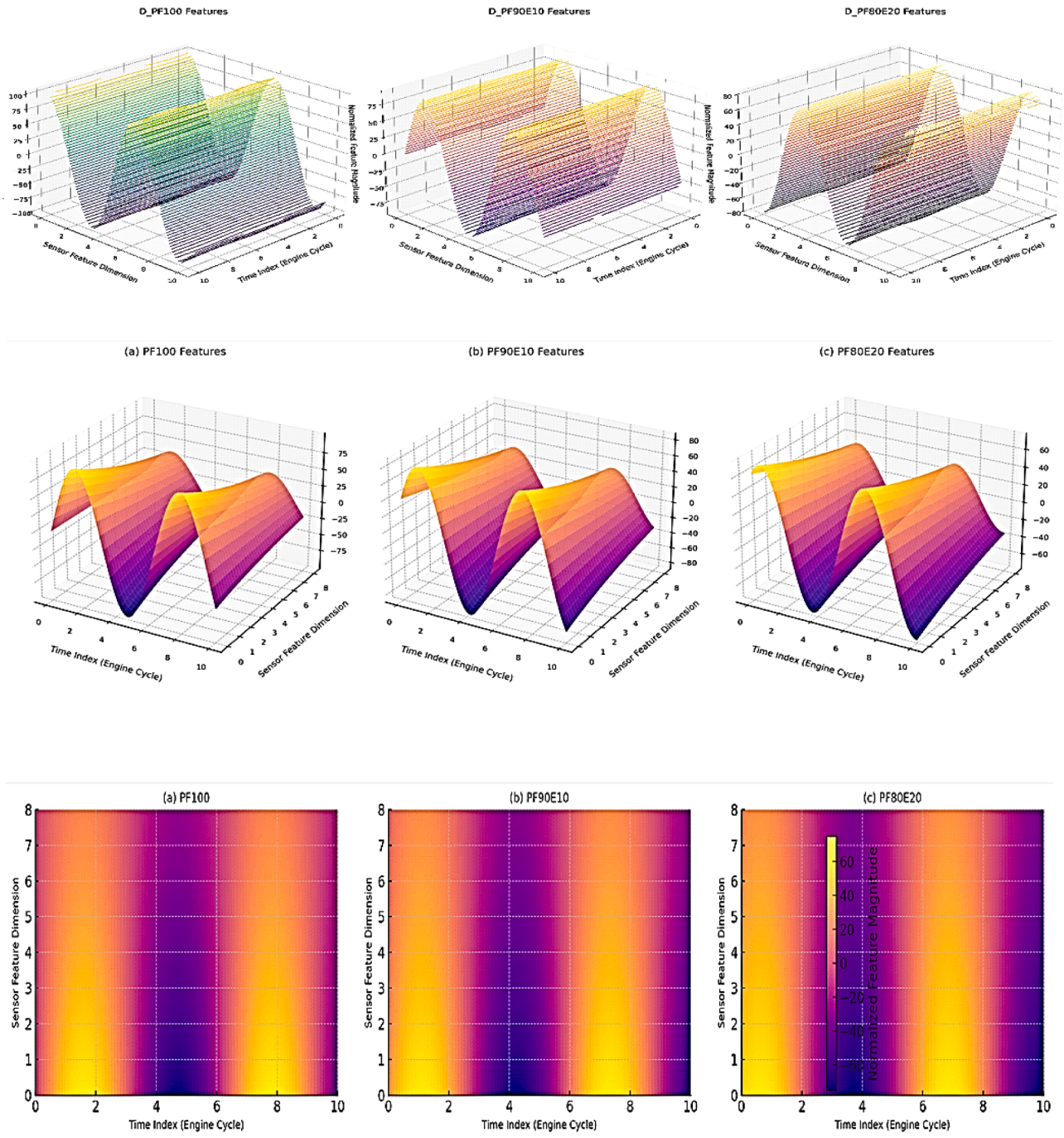

Fig. 11. . Different blend fuels features extraction respectively.

constructed learnt representation features instead of raw high dimensional signals, which greatly minimizes the danger of overfitting and the sample complexity needed for successful learning. Additionally, despite the size of the dataset, the model performs well in terms of generalization, as seen by the good agreement between test set performance and cross validation findings. The claim that the suggested model achieves reliable generalization with the available 1800 samples is supported by the combination of feature-level learning, regularization techniques (e.g., dropout, early stopping, weight decay), and systematic validation, even though larger datasets were always preferred in prior practice. To further increase the model's applicability, we will concentrate on testing it on bigger, multi-source datasets in subsequent work. As shown in Fig. 12, the loss curves demonstrate that the model is robust and well-generalized, with dependable convergence throughout the training procedure. The training and validation MSEs for the FLS model exhibit a quick beginning reduction, with both curves decreasing steeply from around 1.0 to 0.3 during the first ten epochs, demonstrating effective learning from well-initialized weights and relevant features. As the training progressed, the curves stabilized, gradually decaying and converging to a small range between 0.05 and 0.07 MSE, with very tiny changes in the validation loss indicating healthy data variance and no symptoms of overfitting. From epoch 35 onwards, both losses plateaued at the low range of 0.01-0.03 MSE, indicating that the model had reached its maximum capacity given the dataset and architecture. Critically, the persistent overlap of the training and validation curves beyond epoch 30 confirms the absence of overfitting, highlighting good generalization achieved via suitable regularization, cautious feature scaling, and well-calibrated model complexity.

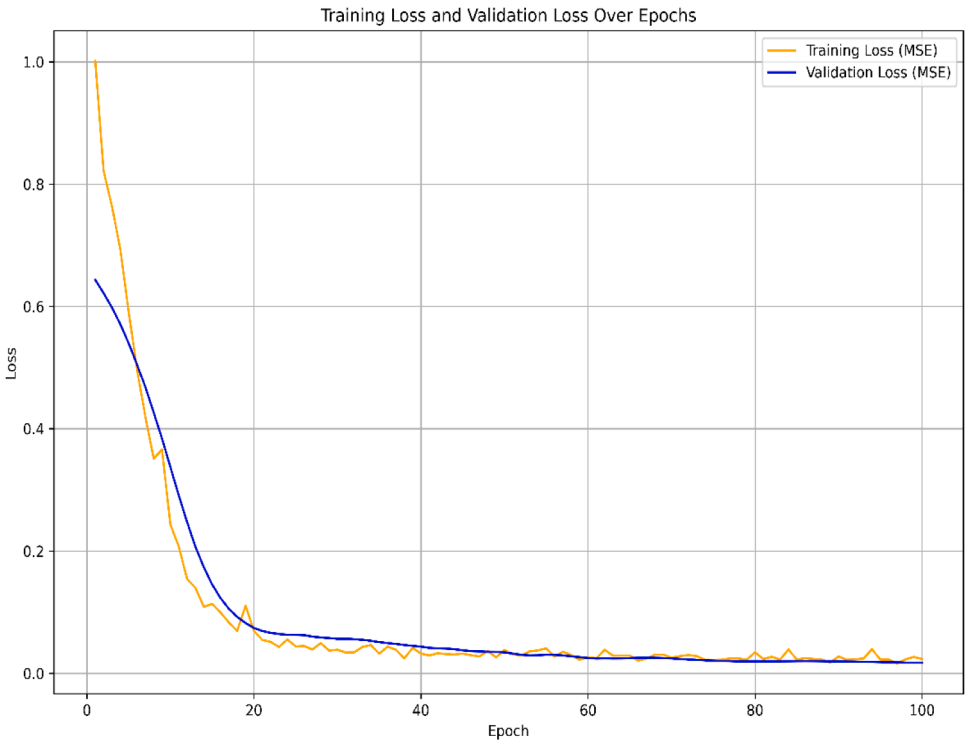

Fig. 12. FSL Model training and validation.

The embedding dimension of 64 was chosen to give a suitably rich latent space for capturing complicated, non-linear feature interactions while avoiding over parameterization. The training regimen used a 100-epoch setup, which directly simulated the low-data inference condition throughout the learning phase. We used the Adam optimizer with an initial learning rate of 0.001 to achieve stable convergence, and a ReduceLROnPlateau scheduler to dynamically modify the learning process and avoid local minima. To ensure robust generalization and avoid overfitting, a multifaceted technique was adopted. Architecturally, this involved using a moderate-sized network with a dropout rate of 0.2 within the embedding network to prevent complex neuron co-adaptations. Procedurally, the most important technique was early stopping with a patience of 10 epochs, which was checked on a held-out set of validation tasks and ensured that training stopped whenever the model's generalized performance reached a plateau. Furthermore, we added data-level robustness by applying mild Gaussian noise augmentation to input features during episodic training, requiring the model to acquire noise-invariant representations. Finally, the rigorous train/validation/test split at the task level, rather than merely the sample level, guaranteed that the model's ultimate performance was assessed

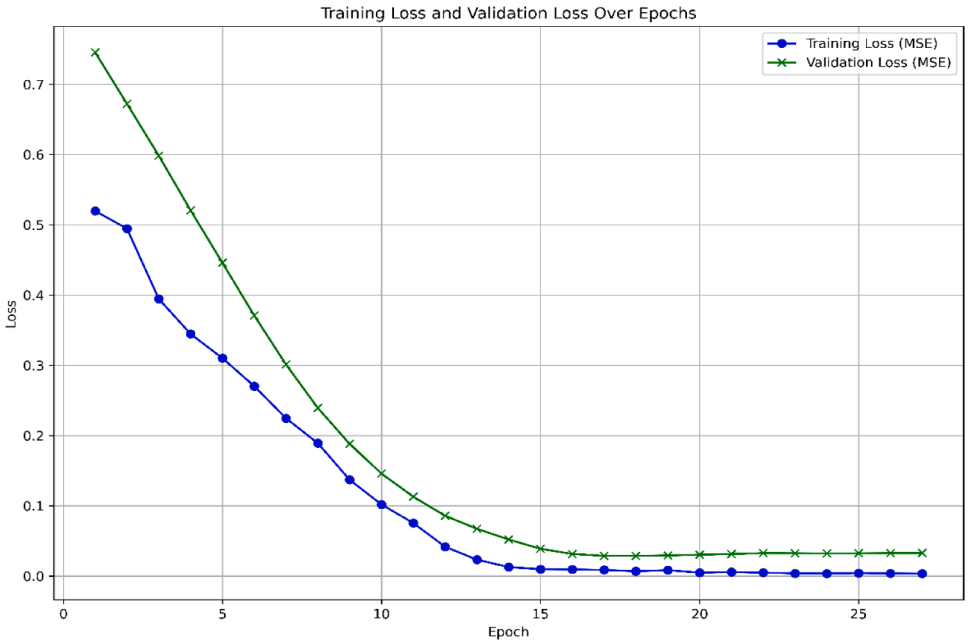

Fig. 13. ANN Model training and validation.

based on its ability to adapt to completely novel blends, providing a real assessment of its generalization capabilities and resistance to overfitting.

The model training and validation results presented in Fig.s 12, 13, and 14, show the performance of three different architectures: FSL, ANN, and CNN. In Fig. 12, the FSL model demonstrates a rapid convergence during the initial epochs, as indicated by the steep decline in the training loss. The training loss consistently decreases, reaching a very low value and stabilizing at around epoch 80. The validation loss closely follows the training loss, confirming that the model is generalizing well and not overfitting. In few-shot learning circumstances, when there is little data available, the FSL model's higher learning efficiency is demonstrated by its ability to achieve low training and validation loss.

Fig. 13 ANN model, in contrast, has a comparable pattern, but with slower convergence in the early epochs. Although the validation loss is still larger than with the FSL model, the training loss drops considerably, suggesting less successful generalization. Indicating either overfitting or slower learning on the validation data, the training loss keeps getting better by epoch 25 but the validation loss reaches a plateau [61]. According to this behavior, the ANN design is successful, but in few-shot circumstances, it needs more epochs or data to function as well as the FSL model.

At last, the CNN model in Fig. 14 shows a comparable loss curve with quick convergence in the early epochs. Like the ANN model, the validation loss still lags behind even if the training loss drops considerably [62]. The CNN model lacks as much improvement in validation loss even with its sophisticated architecture as the FSL model. Especially in few-shot learning situations when data availability is limited, this finding shows the possible advantage of the FSL model in predicting fuel performance and extending outcomes from unseen data in spark ignition engine.

Regarding validation loss and training, the FSL model in SI engine beats the CNN and ANN models. While offering greater generalization and prediction performance for tasks such fuel performance prediction, the fast convergence and low validation loss of the FSL model demonstrate how effectively it manages few-shot learning environments. Although CNN and ANN models both exhibit good performance, the comparison reveals that they would not be able to generalize well in settings with limited data without more data or further modification.

3.8. Actual Vs predicted deposition rate of FSL model

As shown in Fig. 15 the picture compares the actual and predicted values of PF90E10 for the test samples taken from the dataset. The red crosses indicate the expected values; the blue circles reflect the actual values. The close alignment of the two data sets indicates that the model has performed very well in estimating PF90E10′s deposition rate. Particularly between test sample indices 10-20 and 30-40, there are a few small deviations in which the predicted findings vary considerably from the actual ones [63]. Nevertheless, the model may reasonably explain variations in the deposition rate over time as the overall pattern rather nearly matches the actual data. This pattern indicates that the model can estimate future deposition rates with a somewhat high degree of accuracy for practical uses where deposition rates must be expected over lengthy periods of time.

Fig. 16 shows the comparison of the Actual and Predicted values of PF80E20 for the test samples in the dataset. The actual values show as blue circles; the expected values show as red crosses. The results imply that the model may fairly represent the behaviour of the deposition rate for PF80E20 as the expected values fit the general pattern of the real data.

Fig. 17 shows that though there are a few small deviations in some places, especially around test sample indices 10-20 and 30-35, the overall alignment between the actual and expected values indicates that the predictions of the model are very accurate. Little variations in the test dataset or model restrictions might be the cause of these minute changes. Nevertheless, the general great agreement between the actual and expected values suggests that the model is a good fit of deposition rates in this regard. The model is a helpful tool for situations needing exact long-term deposition rate prediction since of its great degree of repeatability.

The actual against predicted values of PF100 for the test samples are compared in the Fig.'s 18 plot. Whereas blue circles represent the actual values, red crosses show the expected values. The graph powerfully shows the great degree of correlation between the actual and expected results as the red crosses tightly follow the blue circles over the complete spectrum of test sample indices.

Though there are a few small differences between the anticipated and actual numbers, both sets of data show pretty similar overall

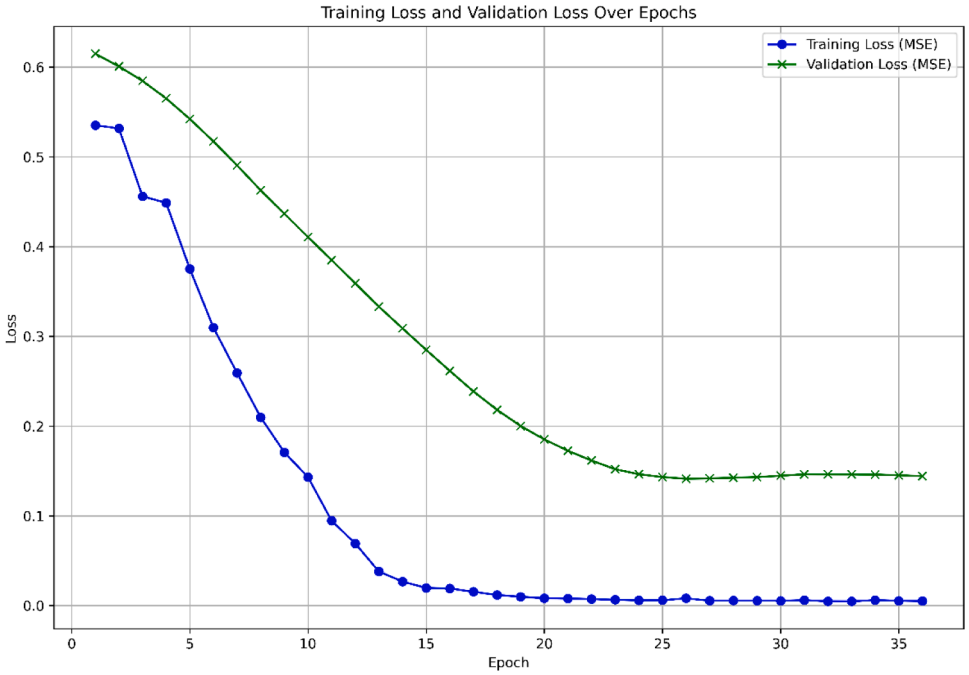

Fig. 14. CNN Model training and validation.

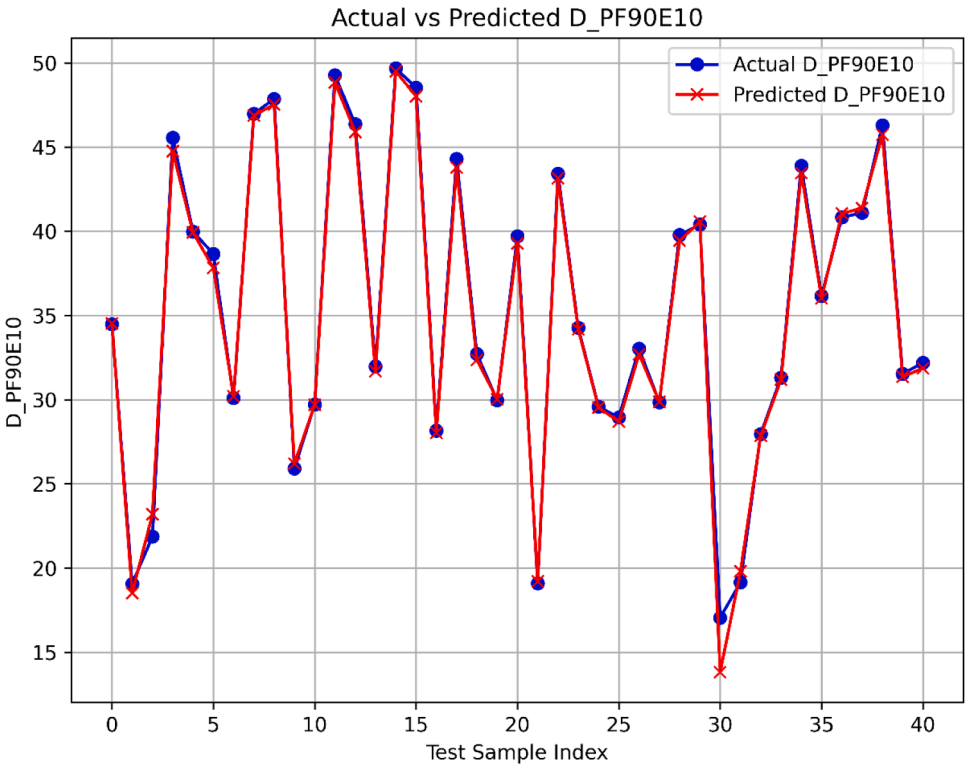

Fig. 15. Actual verses predicted petrol and ethanol PF90E10.

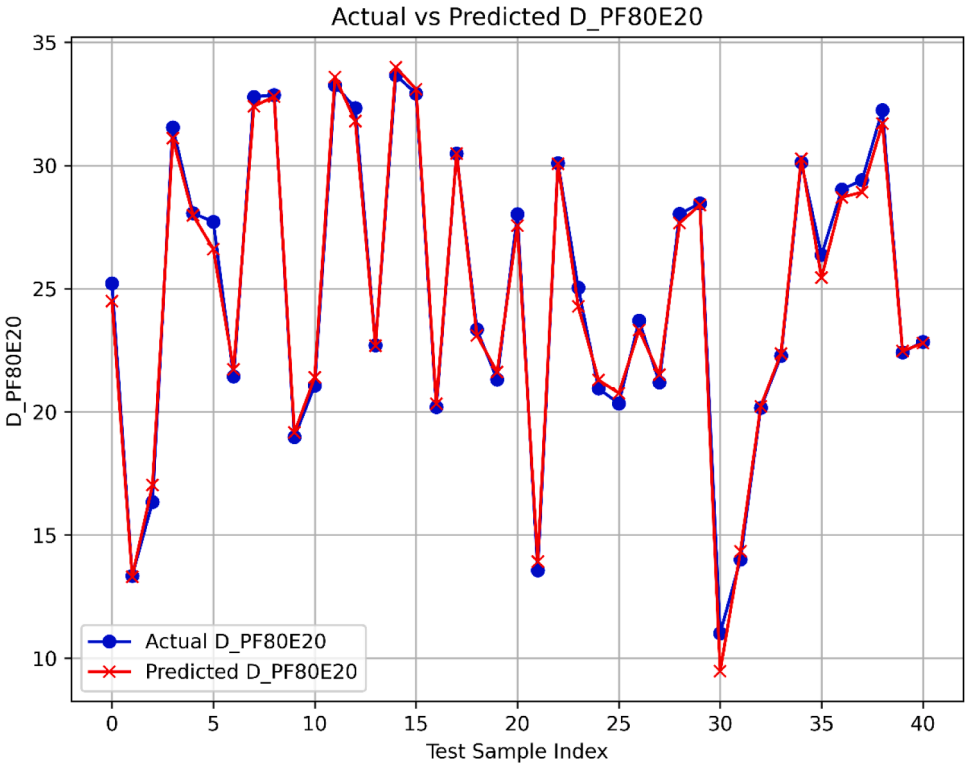

Fig. 16. Actual verses predicted petrol and ethanol PF90E20.

pattern. Little variations in the test set data overlooked by the model or slight overfitting might lead to these effects. With the expected values somewhat closely matching the actual data, the model performs a decent job of portraying the general trend of deposition rates in PF100. This suggests that the model offers consistent forecasts for useful application as it is quite accurate in estimating the deposition rate of PF100 over time.

The Fig. 18 highlights the performance of the CNN model by

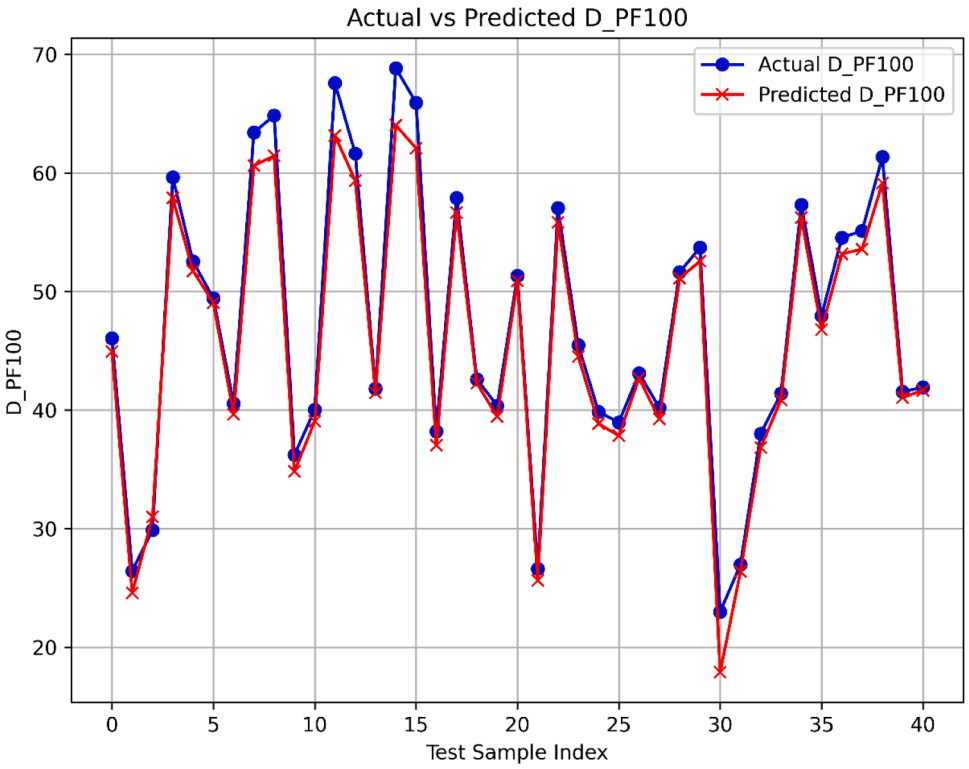

Fig. 17. Actual verses predicted petrol PF100.

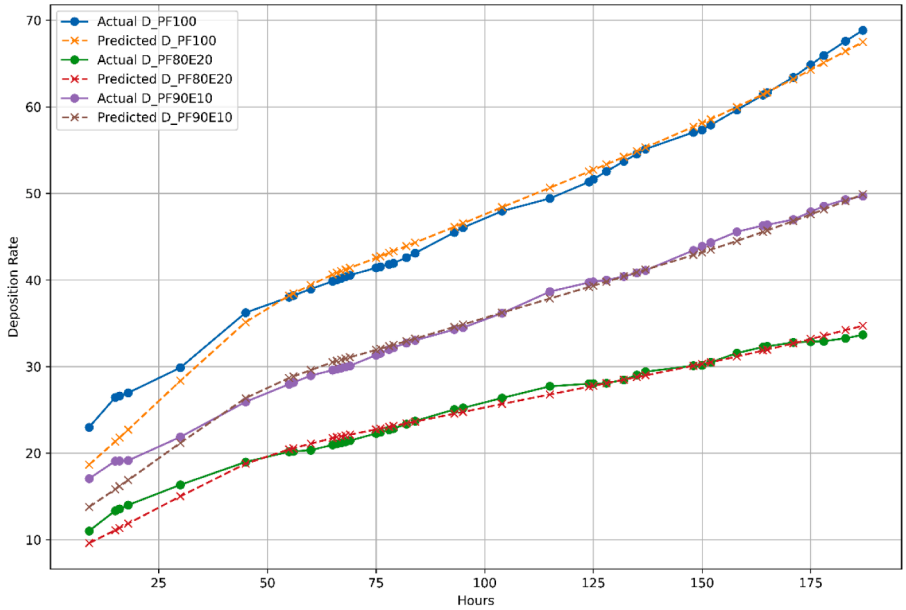

Fig. 18. CNN model actual Vs predicted result for 200 hrs.

comparing the actual and predicted deposition rates for the three fuel blends: PF100, PF80E20, and PF90E10 in spark ignition engine. The solid lines represent the actual deposition rates, while the dashed lines show the predicted values. With the predicted values closely matching the actual data, the CNN model shows a strong fit for the PF100 fuel mix, demonstrating the model's accuracy in predicting deposition rates for this blend. Although significant forecast variations point to possible areas for improvement, especially in capturing finer subtleties of the deposition patterns, the model works rather well for PF80E20. The performance of the model on PF90E10, however, exhibits the most disparity, particularly at later time periods when the expected values deviate from the actual deposition rates.

The CNN model's capacity to generalize is demonstrated by the fact that it accurately depicts the general trend of deposition rates for each of the three fuel mixes. The model predicts the rates for PF80E20 and PF90E10 with notable room for improvement, despite its strong performance for PF100. For certain characteristics or time periods, these disparities may be due to both overfitting and underfitting of the model. Increased training data and hyperparameter tweaking are two more model modifications that might boost accuracy. The CNN model has

potential for forecasting deposition rates across various fuel types in spite of these obstacles, and it may be improved for more accurate forecasts.

For the three petroleum fuel blends PF100, PF80E20, and PF90E10 a comparison of the actual and anticipated deposition rates is shown in ANN Model Results Fig. 19. The projected values are shown by the crosses, while the actual deposition rates are represented by the solid circles. The ANN model does a good job for the PF100 fuel mix; especially in the early part of the observation period, the projected values nearly match the actual data points. Predicted values for PF80E20 similarly show a modest overestimation of the deposition rate, but there are some noticeable variances, especially in the latter hours. The true trend for PF90E10 is difficult for the model to adequately depict, particularly when the deposition rate rises. For this blend, this disparity suggests that the model may not be picking up on certain intricate patterns in the data.

Overall, the ANN model shows promise in forecasting the overall pattern of deposition rates for all three fuel blends; nevertheless, its accuracy in forecasting is limited, especially for PF80E20 and PF90E10. For PF100, where the predicted values deviate from the real data the least, the model works best. However, for the other two fuel types, particularly PF90E10, the model exhibits overfitting or under fitting, suggesting that the accuracy might be increased by modifying the model architecture or training procedure. For the bulk of the time series, the ANN model produces accurate predictions in spite of these problems, demonstrating its applicability for regression tasks in comparable situations.

Two blend fuel mixes, PF100, PF80E20, and PF90E10, are shown in Fig. 20: Few-Shot Learning (FSL) Model Results, which compares the actual and anticipated deposition rates in spark ignition engine. The FSL model has the capacity to forecast deposition rates with a fair degree of precision. The projected and actual readings for the PF100 fuel blend are quite similar, especially during the early hours. There is little deviation from the real pattern of deposition, which the model tracks well. In a similar vein, the model can accurately depict the overall trend for the PF80E20 blend, however there are occasional variations where the predictions tend to differ somewhat from the actual values, particularly in later time periods.

The FSL model's performance for PF90E10 exhibits the most pronounced disparity. The projected values show some lag in relation to the actual deposition rate, even if they follow the overall trend in spark ignition engine. This could be the result of the blend's restricted data availability, which is a typical problem with few-shot learning tasks. Nevertheless, when it comes to forecasting the general course of deposition rates for all three mixes, the FSL model does a good job. Regression problems seem to be a good fit for the FSL model, particularly when there is a shortage of training data. The findings indicate that with further data or fine-tuning, the model's forecast accuracy for all target mixes might be further increased.

Table 8 and Fig. 21 shows radar chart that there are notable variations in how well the CNN, ANN, and FSL models perform across the target variables (PF100, PF90E10 and PF80E20) in spark ignition engine. With the greatest R-squared (R^2) values and significantly lower Mean Absolute Error (MAE) and Mean Squared Error (MSE) values, FSL performs noticeably better than CNN and ANN, demonstrating exceptional prediction accuracy. For instance, FSL only managed to get an MAE of 0.1567 for PF100, while CNN and ANN achieved far higher MAEs of 74.4607 and 4.3603, respectively. With MSE values for the three objectives of 0.0616, 0.0190, and 0.0354 far lower than those found in the other models FSL also exhibits higher predictive power. CNN and ANN have lower R-squared (R^2) values, indicating less accurate predictions, but FSL has values close to 1, indicating a nearly perfect match. In summary, CNN and ANN fared noticeably worse across all criteria, whereas FSL is the most reliable model for forecasting deposition rates.

The FSL model outperformed the CNN and ANN models in every metric, showing the highest R-squared values and the best capacity to forecast deposition rates with the least amount of error. Compared to CNN and ANN, which performed quite well, FSL is the most reliable model for this dataset, as shown by its significantly better performance, particularly in terms of MAE, MSE, and R-squared.

The CNN, ANN, and FSL models are compared, and the results show that the suggested FSL model performs better in terms of prediction for all fuel blends. The table indicates that the FSL model consistently delivers the lowest error rates, with Mean Squared Errors (MSE) between 0.0190 and 0.0616 and Mean Absolute Errors (MAE) between 0.0851 and 0.1567. Its R2 values are remarkably high (0.9995–0.9996), demonstrating near-perfect agreement with the actual deposition data. While the ANN model performs very poorly, as evidenced by greater MAE and MSE values and lower R^2 scores, especially for the PF100 blend ($R^2 = 0.8447$), the CNN model exhibits respectable accuracy, with MAE values between 0.6007 and 1.1547 and R^2 scores over 0.98. Notably, the FSL model's minimal errors and maximum R2 indicate that it captures the deposition trends for the pure gasoline blend (PF100) with slightly

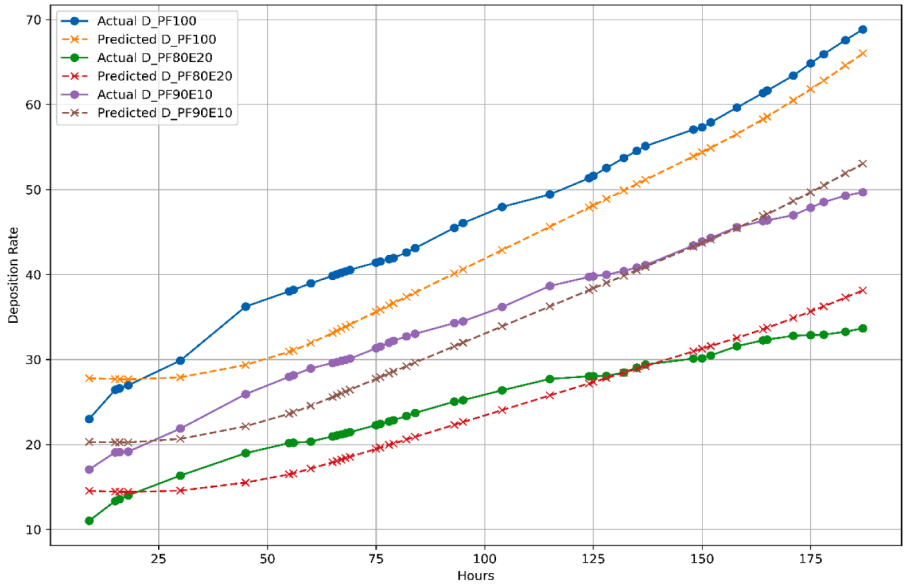

Fig. 19. ANN model actual Vs predicted result for 200 hrs.

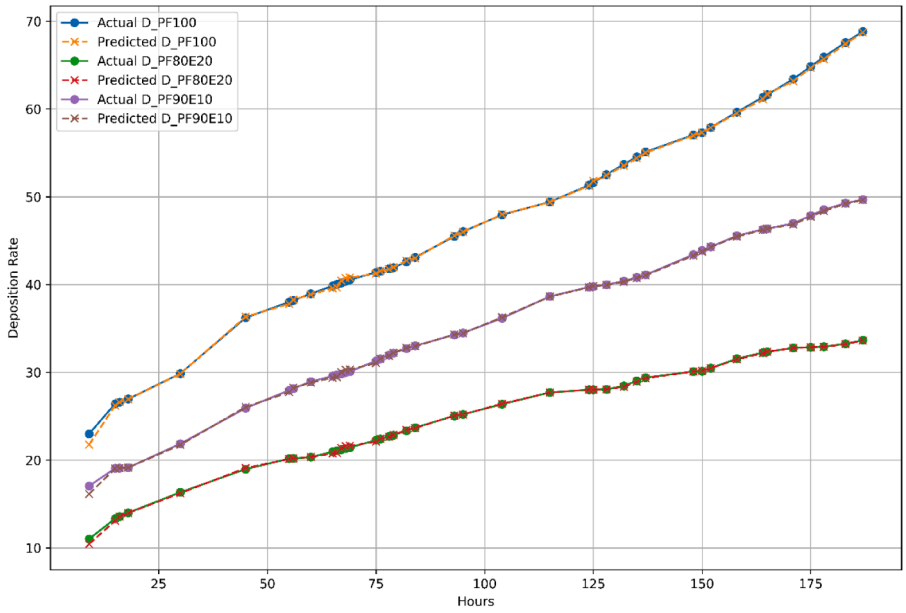

Fig. 20. Few-shot learning (FSL) Model actual vs predicted result for 200 hrs.

Table 8
Performance comparison metrics FSL with ANN, CNN models.

Model	Target	Mean Absolute Error MAE	Mean Square Error MSE	R^2
CNN	PF100	74.4607	8984.4260	0.9822
	PF90E10	34.6129	2663.2011	0.9908
	PF80E20	32.0503	2046.9263	0.9844
ANN	PF100	4.3603	22.0922	0. 8447
	PF90E10	2.2820	7.2365	0.9115
	PF80E20	2.1526	6.0602	0. 8352
FSL	PF100	0.1567	0.0616	0.9996
	PF90E10	0.1164	0.0354	0.9996
	PF80E20	0.0851	0.0190	0.9950

more accuracy than the ethanol-gasoline blends. Overall, this table shows that the FSL model outperforms both traditional CNN and ANN methods as a highly dependable and resilient tool for precisely predicting deposit development over a range of fuel mixtures.

This study analyzed engine wear and spark ignition sound emissions from PF90E10 and PF80E20 gasoline mixtures, unlike PF100. Engine noise emissions, spark plug deposits, and fuel behavior were tested during a 200-hour endurance test. CNN, ANN, and FSL could forecast deposition rates over time, revealing the relationship between engine performance and fuel types [64].

The trial's most significant conclusion was that spark plug nap deposits were observed on PF100, PF90E10, and PF80E20 test fuels. PF80E20 has fewer deposits on its spark plugs than PF90E10 and PF100. The CNN and ANN models found that the PF80E20 combination reduced deposition rates with time. Consistent with the finding. Based on the FSL model, the PF80E20 was projected to have lower deposition rates, which means it is ideal for engine maintenance since spark plugs need to be cleaned or changed more often.

SEM and EDS tests demonstrated large differences in fuel deposition patterns after the endurance test. PF80E20 has fewer spark plug carbon deposits than PF90E10. The carbon concentration of PF100 rose around the spark plug nap, where deposits were thicker and overlapped [49]. The CNN and ANN models predicted greater deposition rates with PF100 compared with PF80E20. Low PF80E20 deposition was predicted using FSL models, which worked better with less data.

Fuel oxygen concentration affects combustion efficiency and emissions during engine noise emission testing. PF90E10 and PF80E20 were quieter than PF100. These binary mixtures' greater oxygen content decreased ignition delay and enhanced combustion efficiency. These attributes directly reduced engine noise [65]. Consistent with their better combustion efficiency and more smooth engine running, the CNN and ANN models showed that PF90E10 and PF80E20 lowered noise emissions over time. Using binary mixes instead of ethanol/gasoline showed a significant decrease in engine noise by generating correct predictions about sound emissions when lacking sufficient data.

In the field of machine learning models, the CNN and ANN models showed great ability in trend in noise emission and deposition rate prediction in SI engine. However, the FSL model proved particularly useful in few-shot scenarios, where limited data is provided. This was particularly relevant for estimating deposition rates as the FSL model possessed notable generalization abilities while trained with fewer data points. Combining CNN's feature extraction, ANN's regression-based approach, FSL's few-shot learning capabilities, and noise emissions and engine wear forecasts, yields effective analysis of fuel types and their effects on engine components.

The study unequivocally demonstrated in total the advantages of using PF90E10 and PF80E20 in reducing engine wear, carbon deposits, and noise emissions as compared to PF100. Particularly crucial in modeling and projecting how different fuels will impact engine performance were the FSL, CNN, and ANN machine learning models. These models helped us to effectively anticipate engine performance given limited data, hence advancing our knowledge of fuel effects. Future studies can focus on enhancing these models even further to maximize fuel compositions for higher engine efficiency and sustainability.

4. Conclusion

A single-cylinder air-cooled horizontal gasoline engine using petroleum fuel PF100, PF90E10, and PF80E20 fuels has been used to evaluate the deposit formation and sound emission of SI engines. Ethanol was added to gasoline blends to improve their stability and solubility. The engine ran faultlessly and smoothly during the test, and the physical and chemical characteristics of binary blend ethanol-gasoline PF80E20 indicated strong potential for use in SI engines. SEM and EDS studies confirmed that PF80E20 produced spark plugs with reduced carbon content, hence extending engine lifetime and lowering maintenance requirements.

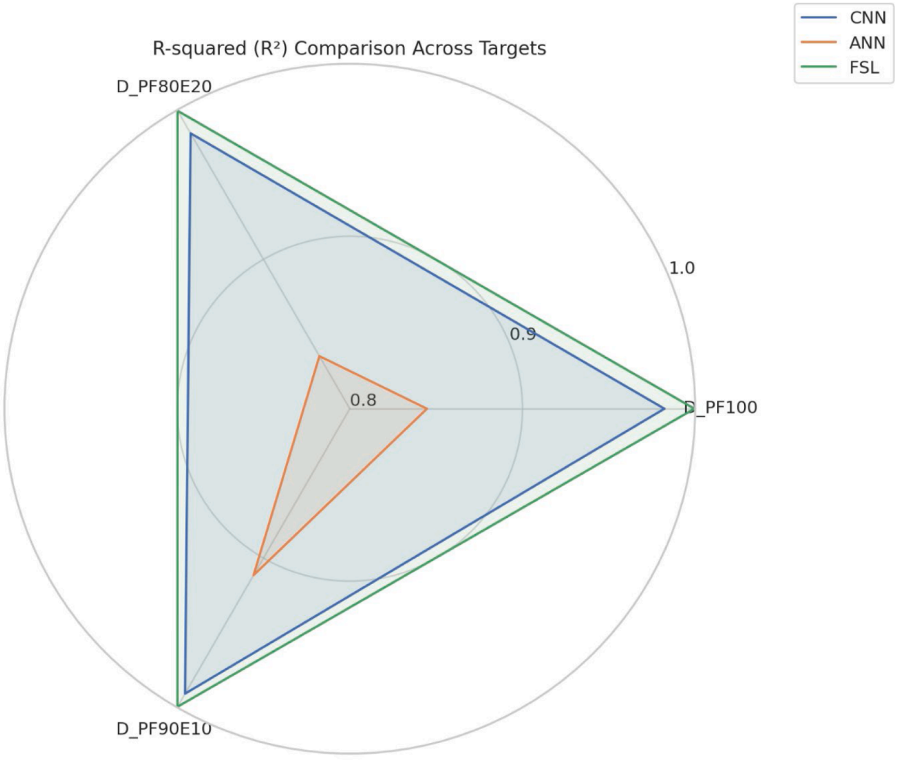

Fig. 21. Rader chart FSL ANN and CNN comparison.

- The baseline fuel PF100 spark plug has more wear overall than the petroleum fuel-ethanol engine and binary blend fuels, according to SEM micrographs and various roughness measurements.
- Engine trial research indicates that PF80E20 is a suitable partial biofuel petroleum fuel substitute. The carbon deposition rate of ethanol-petroleum fuel binary mix fuel was found to be lower than that of baseline fuel (71.15% for PF100, 51.09% for PF90E10, and 34.57% for PF80E20).
- Additionally, the existing spark ignition engine can be readily modified to run on ethanol-gasoline without requiring major internal component modifications. Due to a variety of factors, including a higher oxygen content, ethanol's higher-octane rating enhances knock suppression, leading to more stable combustion and fewer pressure oscillations, blend fuel produced lower sound levels than baseline fuel.
- The ethanol concentration 20% PF80E20 produced the least noise. Consequently, since PF90E10 and PF80E20 not only improved engine performance but also helped to operate the engines quietly, thus they are more environmentally friendly.
- The model outperformed traditional methods such as Artificial Neural Networks (ANN) and Convolutional Neural Networks (CNN), with a training loss of 0.0294 and validation loss of 0.0258, compared to ANN's training loss of 0.0054 (validation loss 0.1452) and CNN's training loss of 0.0037 (validation loss 0.0326), demonstrating its superior efficiency in fuel performance prediction.
- As a result, FSL offers a realistic and gradually deployable solution for real-world predictive maintenance in aerospace, automotive, and smart manufacturing contexts where unique fault patterns arise on a regular basis and quick, cost-effective model adaptation is required.
- This study suggests that PF90E10 and PF80E20 are good fuel replacements for lowering engine wear, noise pollution, and combustion efficiency. By using machine learning models, which also improved fuel performance projection accuracy, future fuel formulation and engine design improvement opportunities were made viable.

4.1. Limitations of the proposed FSL framework

First, because there are so few labeled examples available for each class, possible overfitting is an inherent problem with FSL. The model may still overfit to the support set even while episodic meta-training enhances generalization, especially in cases where samples are noisy or not entirely representative of the underlying data distribution. When sophisticated deep feature extractors are used, this danger is increased even more since they could learn resilient and transferable representations instead of memorizing task-specific patterns. Second, model dependability is greatly impacted by domain shift problems. The FSL framework makes the assumption that the target tasks and meta-training tasks come from comparable distributions. Variations in operating circumstances, sensor qualities, load, or ambient noise might result in significant domain mismatch in practical applications like industrial defect detection or real-world deployment. Performance may suffer in such circumstances as the learnt metric space or prototypes may no longer be discriminative. This restricts the model's direct application across various computers, operating systems, or datasets in the absence of further domain adaption. Third, restricted interpretability of the model is still an issue. The majority of FSL techniques rely on latent embeddings acquired using deep neural networks or distance-based similarity metrics. These representations are useful for categorization, but they don't provide much information about the physical or causative elements that underlie the predictions. In safety-critical systems where decision justification and explain ability are crucial, this lack of transparency can erode user confidence and impede adoption. Although the current FSL model performs well overall in low-data regimes, future research should focus on overfitting, domain generalization, and interpretability.

4.2. Recommendation for future work

Future study should look into creating larger, multi-platform, multi-condition engine datasets to test the model across wider operational

regimes in order to extend this line of inquiry. Furthermore, the transferability and stability of feature representations could be greatly improved by including next-generation pretrained time-series foundation models. The creation of a real-time FSL model that can continuously learn from streaming engine data is another exciting avenue. Lastly, adding dependability measures and uncertainty quantification would make FSL-based methods more appropriate for safety-critical applications in the automotive, power-generation, and aviation industries. Together, these suggestions offer a clear path forward for expanding current research and enhancing the useful implementation of FSL in intelligent engine diagnostics.

Data availability

Data will be made available on request.

CRediT authorship contribution statement

Ali Murtaza Ansari: Writing – review & editing, Writing – original draft, Methodology, Investigation, Data curation, Conceptualization. **Faheem Ahmed Solangi:** Validation, Supervision, Methodology, Formal analysis. **Ali Nawaz Sanjrani:** Writing – review & editing, Writing – original draft, Software, Investigation, Data curation. **Fayaz Hussain:** Writing – original draft, Visualization, Validation, Supervision, Project administration, Conceptualization. **Bo Zhang:** Writing – review & editing, Writing – original draft, Visualization, Validation, Resources, Project administration, Investigation, Funding acquisition. **Zhou Ding:** Writing – review & editing, Writing – original draft, Investigation, Data curation. **Nazmi Mat Nawi:** Writing – review & editing, Writing – original draft, Supervision, Formal analysis.

Declaration of competing interest

The authors declare that they have no known competing financial interests or personal relationships that could have appeared to influence the work reported in this paper.

Acknowledgments

This work was supported by the Natural Science Foundation of Ningxia under Grant No. 2022AAC02003.

References

[1] A.M. Ansari, L.A. Memon, F.A. Solangi, M.T. Ghannam, M.Y.E. Selim, Influence of alcohol blend fuels on performance and noise emission in spark ignition engine, Int. J. Thermofluids 26 (2025) 101120, https://doi.org/10.1016/j.ijft.2025.101120.

[2] L. Fang, X. Zhang, Y. Li, Effect of machine learning algorithms on prediction of in-cylinder combustion pressure of ammonia–oxygen in a constant-volume combustion chamber, Energies 17 (3) (2024) 746. Available: https://www.mdpi.com/1996-1073/17/3/746.

[3] Q. Huang, R. Yang, J. Liu, T. Xie, M. Yang, J. Liu, CFD-based investigation of ammonia combustion and slip behavior in an ammonia-diesel dual-fuel engine, J. Energy Inst. 122 (2025) 102217, https://doi.org/10.1016/j.joei.2025.102217.

[4] Q. Huang, T. Xie, J. Liu, Machine learning-assisted reconstruction of in-cylinder pressure in internal combustion engines under unmeasured operating conditions, Energies 18 (19) (2025) 5235. Available: https://www.mdpi.com/1996-1073/18/19/5235.

[5] F. Xie, R. Chen, L. Zhang, Research on the effects of negative valve overlap duration on the combustion and emission of methanol, ethanol, isopropanol, and n-butanol in a spark induced compression ignition (SICI) engine by experiments and Artificial neural networks, Fuel Process. Technol. 269 (2025) 108190, https://doi.org/10.1016/j.fuproc.2025.108190.

[6] D. Xiongbo, M.C. Lai, M. Jansons, G. Guo, J. Liu, A review of controlling strategies of the ignition timing and combustion phase in homogeneous charge compression ignition (HCCI) engine, Fuel 285 (2021) 119142, https://doi.org/10.1016/j.fuel.2020.119142.

[7] Q. Huang, J. Liu, Preliminary assessment of the potential for rapid combustion of pure ammonia in engine cylinders using the multiple spark ignition strategy, Int. J. Hydrog. Energy 55 (2024) 375–385, https://doi.org/10.1016/j.ijhydene.2023.11.136.

[8] S. Farooq, D. Vinay Kumar, Experimental investigation of gasoline ethanol methanol iso-stoichiometric blends on SI engine, Mater. Today: Proc. (2023), https://doi.org/10.1016/j.matpr.2023.06.138.

[9] R. Yang, J. Liu, J. Liu, Investigation of the formation mechanisms of nitrogen-based pollutants in ammonia-diesel dual-fuel engines by decoupling dilution, thermal, and kinetic effects, J. Energy Inst. 120 (2025) 102125, https://doi.org/10.1016/j.joei.2025.102125.

[10] Y. Yan, T. Xie, J. Liu, Rapid and accurate prediction of molecular dynamics simulations using physics-informed LSTM networks in engine emission analysis: a case study of C3H6/NH3 pyrolysis for PAH formation, J. Energy Inst. 120 (2025) 102090, https://doi.org/10.1016/j.joei.2025.102090.

[11] G. Dhamodaran, G. Esakkimuthu, T. Palani, A. Sundaraganesan, Reducing gasoline engine emissions using novel bio-based oxygenates: a review, Emergent Mater. 6 (2023) 1–21, https://doi.org/10.1007/s42247-023-00470-7.

[12] J. Benajes, G. Antonio, J. Monsalve-Serrano, M. Guzmán, A review on low carbon fuels for road vehicles: the good, the bad and the energy potential for the transport sector, Fuel 361 (2024) 130647, https://doi.org/10.1016/j.fuel.2023.130647.

[13] T. Palani, G. Dhamodaran, G. Esakkimuthu, S. Seetharaman, Experimental study on dual oxygenates (ethanol, n-butanol) with gasoline on MPFI engine performance and emission characteristics, Int. J. Environ. Sci. Technol. (2023), https://doi.org/10.1007/s13762-023-04852-6.

[14] G. Dhamodaran, G. Esakkimuthu, Experimental measurement of physico-chemical properties of oxygenate (DIPE) blended gasoline, Measurement 134 (2018), https://doi.org/10.1016/j.measurement.2018.10.077.

[15] C.S. Lim, J.H. Lim, J.S. Cha, J.Y. Lim, Comparative effects of oxygenates-gasoline blended fuels on the exhaust emissions in gasoline-powered vehicles, J. Environ. Manag. 239 (2019) 103–113, https://doi.org/10.1016/j.jenvman.2019.03.039.

[16] Y. Hua, X. Xiang, Y. Qian, S. Meng, B. Ye, Effect of diffusion oxygen enrichment on soot formation in coflow diffusion flames of gasoline-surrogate fuel doped with ethanol, Fuel 328 (2022) 125306, https://doi.org/10.1016/j.fuel.2022.125306.

[17] N. Rahmat, A.Z. Abdullah, A.R. Mohamed, Recent progress on innovative and potential technologies for glycerol transformation into fuel additives: a critical review, Renew. Sustain. Energy Rev. 14 (3) (2010) 987–1000, https://doi.org/10.1016/j.rser.2009.11.010.

[18] H. Yaman, M. Yesilyurt, S. Uslu, Simultaneous optimization of multiple engine parameters of a 1-heptanol/gasoline fuel blends operated a port-fuel injection spark-ignition engine using response surface methodology approach, Energy 238 (2021) 122019, https://doi.org/10.1016/j.energy.2021.122019.

[19] M.K. Mohammed, H.H. Balla, Z.M.H. Al-Dulaimi, Z.S. Kareem, M.S. Al-Zuhairy, Effect of ethanol-gasoline blends on SI engine performance and emissions, Case Stud. Therm. Eng. 25 (2021) 100891, https://doi.org/10.1016/j.csite.2021.100891.

[20] D.Y. Dhande, N. Sinaga, K.B. Dahe, Study on combustion, performance and exhaust emissions of bioethanol-gasoline blended spark ignition engine, Heliyon 7 (3) (2021) e06380, https://doi.org/10.1016/j.heliyon.2021.e06380.

[21] M. Ilhak, R. Doğan, S. Akansu, N. Kahraman, Experimental study on an SI engine fueled by gasoline, ethanol and acetylene at partial loads, Fuel 261 (2020) 116148, https://doi.org/10.1016/j.fuel.2019.116148.

[22] G. Kushwaha, S. Saraswati, B. Paul, Characterisation of spark plug deposits of an SI engine fuelled with gasoline-ethanol blends, Int. J. Ambient Energy 43 (1) (2022) 5309–5317, https://doi.org/10.1080/01430750.2021.1946142.

[23] S. Di Iorio, F. Catapano, A. Magno, P. Sementa, B.M. Vaglieco, The potential of ethanol/methanol blends as renewable fuels for DI SI engines, Energies 16 (6) (2023) 2791. Available: https://www.mdpi.com/1996-1073/16/6/2791.

[24] F. Catapano, S. Di Iorio, A. Magno, P. Sementa, B.M. Vaglieco, Effect of ethanol blends, E10, E25 and E85 on sub-23 nm particle emissions and their volatile fraction at exhaust of a high-performance GDI engine over the WLTC, Fuel 327 (2022) 125184, https://doi.org/10.1016/j.fuel.2022.125184.

[25] F. Szwajca, Z. Stepien, I. Pielecha, The influence of alcohol-gasoline blends and deposit control additives on fuel injector contamination in SI DI engines, Combust. Engines 202 (2025), https://doi.org/10.19206/CE-207120.

[26] T. Dinh Xuan, D. Vu Minh, B.P. Hoa, K.N. Duc, V. Nguyen Duy, Influence of ethanol-gasoline blended fuel on performance and emission characteristics of the test motorcycle engine, J. Air Waste Manag. Assoc. 72 (8) (2022) 895–904, https://doi.org/10.1080/10962247.2022.2064003.

[27] M. Usman, F. Ali, A. Khan, et al., Comparative assessment of ethanol and methanol–ethanol blends with gasoline in si engine for sustainable development, Sustainability 15 (9) (2023) 7601. Available: https://www.mdpi.com/2071-1050/15/9/7601.

[28] P. Ding, M. Jia, X. Zhao, Meta deep learning based rotating machinery health prognostics toward few-shot prognostics, Appl. Soft Comput. 104 (2021) 107211, https://doi.org/10.1016/j.asoc.2021.107211.

[29] Y. Zhao, Y. Sun, L. Jiang, R. Yang, Few-shot learning for prescriptive maintenance, 2022, pp. 404-406.

[30] Y. Shi, Y. Cao, Y. Chen, L. Zhang, Meta learning based residual network for industrial production quality prediction with limited data, Sci. Rep. 14 (2024), https://doi.org/10.1038/s41598-024-62174-0.

[31] M. Balat, Production of bioethanol from lignocellulosic materials via the biochemical pathway: a review, Energy Convers. Manag. 52 (2) (2011) 858–875, https://doi.org/10.1016/j.enconman.2010.08.013.

[32] S. Kumar, J. Cho, J. Park, I. Moon, Advances in diesel–alcohol blends and their effects on the performance and emissions of diesel engines, Renew. Sustain. Energy Rev. 22 (2013) 46–72, https://doi.org/10.1016/j.rser.2013.01.017.

[33] S. Kumar, P. Sharma, K. Pal, Application of machine learning approach in internal combustion engine: a comprehensive review, 2023, pp. 165-178.

[34] L. Shalahuddin, A. Suksmono, Y.Sembiring Depari, Prediction of internal combustion engine performance using artificial intelligence, Maj. Ilm. Pengkaj. Ind. 14 (2020) 153–162, https://doi.org/10.29122/mipi.v14i2.4164.
[35] H. Yu, M. Gao, H. Zhang, Y. Chen, Dynamic modeling for SO2-NOx emission concentration of circulating fluidized bed units based on quantum genetic algorithm - Extreme learning machine, J. Clean. Prod. 324 (2021) 129170, https://doi.org/10.1016/j.jclepro.2021.129170.
[36] Q. Do, S.K. Lo, J.F. Chen, A comparative study of machine learning techniques in prediction of exhaust emissions and performance of a diesel engine fuelled with biodiesel blends, Nat. Environ. Pollut. Technol. 20 (2021), https://doi.org/10.46488/NEPT.2021.v20i02.049.
[37] K. Kayaalp, S. Metlek, Prediction of burning performance and emissions indexes of a turboprop motor with artificial neural network, Aircr. Eng. Aerosp. Technol. 93 (3) (2021) 394–409, https://doi.org/10.1108/aeat-08-2020-0177.
[38] A.M. Liaquat, H.H. Masjuki, M.A. Kalam, I.M. Rizwanul Fattah, Impact of biodiesel blend on injector deposit formation, Energy 72 (2014) 813–823, https://doi.org/10.1016/j.energy.2014.06.006.
[39] G. Kushwaha, S. Saraswati, B. Paul, Characterization of spark plug deposits of an SI engine fuelled with gasoline-ethanol blends, Int. J. Ambient Energy 43 (2021) 1–38, https://doi.org/10.1080/01430750.2021.1946142.
[40] M. Eyidogan, A. Ozsezen, M. Canakci, A. Türkcan, Impact of alcohol–gasoline fuel blends on the performance and combustion characteristics of an SI engine, Fuel 89 (2010) 2713–2720, https://doi.org/10.1016/j.fuel.2010.01.032.
[41] M. Mofijur, et al., Impact of nanoparticle-based fuel additives on biodiesel combustion: an analysis of fuel properties, engine performance, emissions, and combustion characteristics, Energy Convers. Manag. X (2023) 100515, https://doi.org/10.1016/j.ecmx.2023.100515.
[42] M. Koç, Y. Sekmen, T. Topgül, H. Yücesu, The effects of ethanol–unleaded gasoline blends on engine performance and exhaust emissions in a spark-ignition engine, Renew. Energy 34 (2009) 2101–2106, https://doi.org/10.1016/j.renene.2009.01.018.
[43] J. Li, Y. Wenbin, W.M. Yang, Evaluating performance and emissions of a CI engine fueled with n-octanol/diesel and n-butanol/diesel blends under different injection strategies, Fuel 284 (2021) 119085, https://doi.org/10.1016/j.fuel.2020.119085.
[44] S. Sinha, A. Agarwal, Experimental investigation of the effect of biodiesel utilization on lubricating oil degradation and wear of a transportation CIDI engine, J. Eng. Gas Turbines Power 132 (2010), https://doi.org/10.1115/ICEF2007-1721.
[45] A. Ansari, L. Memon, F. Solangi, M. Zulfiqar, N. Sarwar, A. Rab, Investigation of effect of deposit formation on exhaust valve and lubricating oil debris using green alcohol blend fuel in spark ignition engine, J. Kejuruter. 37 (2025) 3735–3742, https://doi.org/10.17576/jkukm-2025-37(8)-07.
[46] G. Shu, L. Dong, X. Liang, A review of experimental studies on deposits in the combustion chambers of internal combustion engines, Int. J. Engine Res. 13 (2012) 357–369, https://doi.org/10.1177/1468087411427661.
[47] U.A. Rajput, et al., Effect of higher alcohol on injector deposit and wear in compression ignition engine, J. Therm. Eng. 11 (3) (2025) 727–739. Available: https://dergipark.org.tr/en/pub/thermal/issue//1700182.
[48] A.T. Hoang, Q.V. Tran, A.R.M.S. Al-Tawaha, V.V. Pham, X.P. Nguyen, Comparative analysis on performance and emission characteristics of an in-Vietnam popular 4-stroke motorcycle engine running on biogasoline and mineral gasoline, Renew. Energy Focus 28 (2019) 47–55, https://doi.org/10.1016/j.ref.2018.11.001.
[49] F. Solangi, et al., Investigation of lubricating oil and exhaust valve deposit formation using blend fuels in CI engine, J. Kejuruter. 37 (2025) 287–298, https://doi.org/10.17576/jkukm-2025-37(1)-19.
[50] I. Konkol, J. Cebula, L. Świerczek, J. Sopa, A. Cenian, Characterization of deposits formed in gas engines fuelled by coal mine methane, Materials 16 (2023) 2517, https://doi.org/10.3390/ma16062517.
[51] A. Ym, M. Arai, Deposition characteristics of diesel and bio-diesel fuels, Fuel 88 (2009) 2163–2170, https://doi.org/10.1016/j.fuel.2009.01.021.
[52] F.A. Solangi, et al., Debris accumulation, acoustic and wear analysis of compression ignition engine using bio alcohols blends, Case Stud. Therm. Eng. 76 (2025) 107408, https://doi.org/10.1016/j.csite.2025.107408.
[53] F. Solangi, et al., Comparative assessment of head deposition, exhaust gas temperature and sound emission in CI engine using blend fuel, J. Kejuruter. 36 (2024) 1321–1327, https://doi.org/10.17576/jkukm-2024-36(3)-40.
[54] A.Z.M. Fathallah, F. Pinto, The Influence of NaCl dissolved on biodiesel of used cooking oil on performance and its degradation of main components of diesel engine, IOP Conf. Ser. 972 (1) (2022) 012030.
[55] A. Agarwal, A. Dhar, Karanja oil utilization in a direct-injection engine by preheating. Part 2: Experimental investigations of engine durability and lubricating oil properties, Proc. Inst. Mech. Eng. D-J. Automob. Eng. 224 (2010) 85–97, https://doi.org/10.1243/09544070JAUTO1267.
[56] X. Li, C. Guan, K. Yang, C.S. Cheung, Z. Huang, Impact of lower and higher alcohol additions to diesel on the combustion and emissions of a direct-injection diesel engine, Environ. Sci. Pollut. Res. 26 (2019), https://doi.org/10.1007/s11356-019-05275-y.
[57] A.M. Ansari, L.A. Memon, M.T. Ghannam, M.Y. Selim, Impact of biodiesel blended fuel with nanoparticles on performance and noise emission in compression ignition engine, Int. J. Thermofluids 19 (2023) 100390.
[58] M. Dandu, K. Nanthagopal, Clean Karanja methyl ester compatibility study on long term tribological behavior of a compression ignition engine, Fuel 291 (2021) 120148, https://doi.org/10.1016/j.fuel.2021.120148.
[59] T. Huu, K. Duc, T. Nguyen, N. Tien, An experimental study on wear, deposits, performance, and emissions of bio-fueled motorcycle engines, Recov. Util. Environ. Eff. 45 (2023) 1309–1320, https://doi.org/10.1080/15567036.2023.2178549.
[60] M.B. Sanjeevannavar, et al., Machine learning prediction and optimization of performance and emissions characteristics of IC engine, Sustainability 15 (18) (2023) 13825. Available: https://www.mdpi.com/2071-1050/15/18/13825.
[61] A.S. El-Shafay, U.F. Alqsair, S.M. Abdel Razek, M.S. Gad, Artificial neural network prediction of performance and emissions of a diesel engine fueled with palm biodiesel, Sci. Rep. 12 (1) (2022) 9286, https://doi.org/10.1038/s41598-022-13413-9.
[62] A. Warey, J. Gao, R.O. Grover, Generalization performance of a deep learning based engine-out emissions model, Energy AI 5 (2021) 100080, https://doi.org/10.1016/j.egyai.2021.100080.
[63] A.N. Sanjrani, et al., High-speed train wheel set bearing analysis: practical approach to maintenance between end of life and useful life extension assessment, Results Eng. 25 (2025) 103696, https://doi.org/10.1016/j.rineng.2024.103696.
[64] M. Ahsan, D. Bismor, P. Fabiś, Comparison of ANN and CNN models for misfire detection in vehicle engine at different RPMs with low-cost ADXL1002 accelerometer, 2024, pp. 60-65.
[65] F. Solangi, L. Memon, S. Samo, M. Luhur, A. Bhutto, A. Ansari, Analysis of lubricant oil degradation and sound pressure level for CI engine using blend fuels, J. Teknol. 86 (2024) 131–137, https://doi.org/10.11113/jurnalteknologi.v86.19756.